

UNIVERSIDAD SAN FRANCISCO DE QUITO USFQ

Colegio de Ciencias e Ingeniería

**Metal Nanosphere Model and graphical
representation of scattered field for
nanoparticles of any size using Mie
Theory**

Nicole Recalde Mora

Física

Trabajo de titulación presentado como requisito
para la obtención del título de

Licenciado en Física

Mayo 15, 2023

UNIVERSIDAD SAN FRANCISCO DE QUITO USFQ

Colegio de Ciencias e Ingeniería

HOJA DE CALIFICACIÓN DE TRABAJO DE FIN DE
CARRERA

Metal Nanosphere Model and graphical
representation of scattered field for
nanoparticles of any size using Mie
Theory

Nicole Recalde Mora

Nombre del profesor, Título académico: Alessandro Veltri, PhD

May 15, 2023

© Derechos de Autor

Por medio del presente documento certifico que he leído todas las Políticas y Manuales de la Universidad San Francisco de Quito USFQ, incluyendo la Política de Propiedad Intelectual USFQ, y estoy de acuerdo con su contenido, por lo que los derechos de propiedad intelectual del presente trabajo quedan sujetos a lo dispuesto en esas Políticas.

Asimismo, autorizo a la USFQ para que realice la digitalización y publicación de este trabajo en el repositorio virtual, de conformidad a lo dispuesto en la Ley Orgánica de Educación Superior del Ecuador.

Nombres y apellidos: Nicole Recalde Mora

Código: 00208946

Cédula de Identidad: 1752483147

Lugar y fecha: Mayo 15, 2023

ACLARACIÓN PARA LA PUBLICACIÓN

Nota: El presente trabajo, en su totalidad o cualquiera de sus partes, no debe ser considerado como una publicación, incluso a pesar de estar disponible sin restricciones a través de un repositorio institucional. Esta declaración se alinea con las prácticas y recomendaciones presentadas por el Committee on Publication Ethics COPE descritas por Barbour et al. (2017) Discussion document on best practice for issues around theses publishing, disponible en <http://bit.ly/COPETheses>

UNPUBLISHED DOCUMENT

Note: The following capstone project is available through Universidad San Francisco de Quito USFQ institutional repository. Nonetheless, this project – in whole or in part – should not be considered a publication. This statement follows the recommendations presented by the Committee on Publication Ethics COPE described by Barbour et al. (2017) Discussion document on best practice for issues around theses publishing available on <http://bit.ly/COPETheses>

Agradecimientos

A mi familia por su apoyo. A mis amigos por todas las memorias bonitas que llevo de la universidad. A mi supervisor Alessandro Veltri por su apoyo y confianza en mi trabajo, y por transmitirme su pasión por la ciencia. A Nina por escuchar y entender. A Nabla por llegar a mi vida, por su compañía durante todas las madrugadas, y por su cariño incondicional siempre.

A mi misma hace cinco años porque a pesar de pensar que no podría, de no entender nada y de lo difícil que se sentía, seguí intentando.

Resumen

El trabajo aquí presentado busca proporcionar un modelo integral del comportamiento de nanopartículas metálicas (mgNPs) de cualquier tamaño sumergidas en medios de ganancia. Mediante el uso de la teoría de Mie, ecuaciones ópticas de Bloch y ecuaciones de Maxwell para condiciones de borde, se logró una caracterización de las polarizabilidades dinámicas y, posteriormente, de los campos electromagnéticos del metal y del medio.

Los resultados obtenidos se validan comparando la polarizabilidad cuasiestática y de Mie. Surgen fenómenos interesantes con los primeros dos coeficientes de Mie de una mgNP de 10 nm con diferentes niveles de ganancia y línea central de emisión dada; en particular, modelado del campo y emisión de modos superiores impulsada por ganancia. Además, se genera una representación gráfica del campo disperso, proporcionando información sobre las características espaciales del sistema.

Palabras clave: *teoría de Mie, polarizabilidad dinámica, modelado de campo, emisión de modos superiores*

Abstract

The work presented here aims provide a comprehensive model of the behaviour of metal nanoparticles (mgNP) of any size submerged in gain media. Through the use of Mie theory, Optical Bloch equations, and Maxwell's equations for boundary conditions, a full characterization of the dynamic polarizabilities and subsequently the electromagnetic fields for both the metal and host were found.

The obtained results are validated by comparison between the quasi-static and Mie Polarizabilities. Interesting phenomena are observed when depicting the first two Mie coefficients in a 10nm mgNP with different levels of gain and a designated emission center-line; namely, field sculpting and higher mode gain-driven emission. Moreover, a graphical representation is generated for the sculpted scattered field, offering insight into the spatial characteristics of the system.

Keywords: *Mie theory, dynamic polarizability, field sculpting, higher-mode emission*

Contents

| | | |
|----------|--------------------------------------|-----------|
| 1 | Introduction | 12 |
| 1.0.1 | An overview of Plasmonics | 12 |
| 1.0.2 | Description of the problem | 14 |
| 2 | Mathematical Modelling | 17 |
| 2.1 | The free electron model | 17 |
| 2.2 | The Gain assisted Medium | 18 |
| 2.2.1 | Normalization | 22 |
| 2.3 | Steady state permittivity | 23 |
| 3 | Mie Theory | 26 |
| 3.1 | Boundary conditions | 31 |

| | |
|--|-----------|
| | 8 |
| 3.1.1 Tangential continuity Electric Field | 32 |
| 3.1.2 Tangential continuity Magnetic Field | 34 |
| 3.2 Time evolution of coefficients | 36 |
| 4 Results | 39 |
| 4.1 Polarizability | 39 |
| 4.2 Mie coefficients | 43 |
| 4.3 Higher mode enhancing | 44 |
| 4.4 Higher mode gain-driven emission | 46 |
| 4.5 Gain driven field sculpting | 47 |
| 5 Discussion | 49 |
| 6 Conclusions | 51 |
| Bibliografía | 51 |
| A Optical Bloch equations | 63 |
| A.1 The operator dipole moment | 65 |

| | |
|---|----|
| | 9 |
| A.2 Polarization of the material | 68 |
| A.2.1 Time evolution of the density matrix | 70 |
| A.3 Code for the temporal evolution of the fields | 72 |

List of Figures

| | | |
|-----|--|----|
| 4.1 | Time evolution and spectra of Polarizability of a 1 nm mgNP | 41 |
| 4.2 | Time evolution and spectra of Polarizability of a 10 nm radius mgNP | 42 |
| 4.3 | Time evolution and spectra for second Mie coefficient of a 10 nm radius mgNP, no gain added with quadrupolar center-line | 43 |
| 4.4 | Time evolution and spectra for Mie coefficients of a 10 nm radius mgNP, gain below emission threshold with quadrupolar center-line . | 45 |
| 4.5 | Time evolution and spectra of second Mie coefficient of a 10 nm radius mgNP, gain beyond emission threshold with quadrupolar center-line | 46 |
| 4.6 | Graphical representation of scattered field through 10 nm mgNP, no gain added | 47 |
| 4.7 | Square modulus of the first two Mie coefficients as a function of G . | 48 |

| | |
|--|----|
| 4.8 Graphical representation of scattered field through 60 nm mgNP, gain added with quadrupolar emission centerline | 48 |
|--|----|

Chapter 1

Introduction

1.0.1 An overview of Plasmonics

The physical foundation of the LASER ¹ and, as we will later discover, the SPASER ², lies in the ability to undergo stimulated emission of electromagnetic radiation and to support a large number of vibrational modes. To achieve this, the material used must possess the capability to oscillate collectively.

Plasmons are among the most collective and coherent material oscillations observed in nature [1]. They arise in bulk materials when a plasma (a gas of charged particles) responds collectively to electromagnetic fields. Therefore, delving into the definition of the SPASER requires us to venture into the realm of Plasmonics.

¹Light Amplification by Stimulated Emission of Radiation

²Surface Plasmon Amplification by Stimulated Emission of Radiation

Plasmonics is an interdisciplinary field that explores the interaction between light and conduction electrons in metal nanostructures. It combines principles from Optics, Quantum Mechanics, Solid-state Physics, and Nanotechnology [2]. In recent years, Plasmonics has gained significant attention due to its applications in various fields such as medicine [3], energy harvesting, and novel optical media. Although there are still challenges to be addressed, plasmon related phenomena are already on the fast track to becoming cornerstones of future technologies: this is, to a large extent, due to the versatility of plasmonic circuits which show a limited heat dispersion compared with their electronic counterpart while sharing with the photonic integrated ones the capability to directly process light signals [1]. Plasmonic circuits are thus able to integrate the data capacity, speed and thermal efficiency of Photonics with the size optimization of Electronics.

As mentioned above, in fact, Surface Plasmons (SP) are collective plasma oscillations that occur at the interface between two materials, normally a metal and a dielectric, when the incident electromagnetic wave couples with the metal's free electrons creating a coherent oscillation which produces a strong and strictly confined electromagnetic field enhancement [4]. This way a SP allows to compress the frequency and phase information of the impinging field to a region of space much smaller than the exciting wavelength, functionally overcoming the size restriction the diffraction limit imposes on photonic devices.

The Surface Plasmons we will discuss in this work are Localized Surface Plasmons (LSP) [5–7]. LSP's are non propagating SP's confined to a nanoscale metallic structure or nanoparticle (NP). Nanoparticles with different geometries can exhibit

different LSP modes, however the mechanism supporting the characteristic LSP's high field enhancement [8] at a specific frequency range, is always related to the interaction between the frequency-dependent index of refraction of the chosen metal and the one of the dielectric around it. Typically, the used NP is smaller than the wavelength of the incident field so that its scattered field results in a very localized and more intense copy of the impinging one.

1.0.2 Description of the problem

In the study we present here we have chosen a metal sphere as the LSP supporting nanoparticle. Spherical particles have been the unsung heroes of the theoretical understanding of LSP since its very beginning [9–14] and they are still helping to unravel novel phenomena [15–21], given that their symmetry simplifies modelling while withholding most of the relevant details. Moreover they are thermally stable [22–28] and obtainable in large numbers via nanochemical synthesis [28–34].

Gain media such as laser dyes, semiconductor quantum dots [35], and rare-earth are often used in laser systems, optical amplifiers, and other photonic devices [36] because of their ability to amplify an input signal (usually an optical signal) by transferring energy from an external source (such as an optical pump) into the medium itself. This amplification is achieved through a process called stimulated emission, in which an excited atom or molecule in the gain medium emits a photon that is in phase with the incoming signal, resulting in an amplification of the original signal [37–40].

In the context of plasmonic nanoparticles, gain media can be used to amplify the plasmonic response of the nanoparticle [41–50], and beyond a certain *gain threshold* to allow the doped NP to support a LSP even without an external exciting field. The resulting “emitted” plasmonic field arising from the interplay between the emission center line of the used gain material and the resonant frequency of the plasmonic NP can (under certain circumstances) be very narrow. This phenomenon mimics, on numerous levels, a LASER and, for this reason was dubbed SPASER in the article where its theoretical possibility was first mentioned [51]. Since then, this flamboyant new idea moved from a controversial hypothesis [35, 52] to an experimental reality [3, 53, 54] and is now finding its way to real life applications [55–57].

A widely used and accepted model for gain assisted metal nanoparticles consists of describing the steady state polarizability of the nanoparticle using a Lorentzian model for the gain permittivity and a Drude model for the permittivity of metal [48, 49, 58–62]. The limits of this approach have already been evidenced in a previous work [63], where it has been demonstrated how this steady state approach correctly describes the system only when a quantity of gain below a threshold is involved. When higher gain levels are introduced in the system, the structure begins to emit and the steady state approach fails. In the same work, a more complex time-dynamical approach able to handle the emissive regime was introduced for the first time. However, that preliminary analysis was limited to the quasi-static limit (where the size of the nanoparticle is much smaller than the exciting wavelength).

In this thesis, we present a theoretical description of the same system, this

time transcending any particle size limit by means of a time-dynamic Mie theory able to capture the most fascinating aspects of the problem. This new and original approach allows us, in principle, to follow the evolution in time of any of the infinite multipolar resonances in the scattered electromagnetic field of a mgNP. Moreover, by including a technique derived from the Optical Bloch equations, this model also allows us to describe the interplay between the chosen gain element and the time evolution of each multipolar resonance. In what follows, we will validate the results of this model by comparing them with the ones obtained with the quasi-static approach presented in [63]. We will then provide a novel characterization that was out of reach without the extension presented here and use it to identify a relation between the steady state behavior of a mode with the possibility to turn it into an electromagnetic emitter. Finally, as a working example of the wide range of novel characterizations this method can allow, we will demonstrate how it is possible (by choosing the right gain emission center-line) to inject energy in a weak/higher mode, effectively “sculpting” the shape of the resulting scattered field.

Chapter 2

Mathematical Modelling

2.1 The free electron model

By Coulomb's and Newton's second law, the interaction of the electrons inside the metal with the electric field can be modelled as:

$$\frac{d^2\mathbf{r}}{dt^2} + 2\gamma\frac{d\mathbf{r}}{dt} = \frac{e}{m_e}\mathbf{E}_m \quad (2.1)$$

\mathbf{r} : displacement of the electron cloud with respect to equilibrium;

γ : collisions friction coefficient; e : charge of electron; m_e : mass of the electron.

The polarization of the metal attributed to the displacement of charges with number density n_e is $\mathbf{\Pi}_m = n_e e \mathbf{r}$, so 2.1 becomes

$$\left(\frac{d^2}{dt^2} + 2\gamma\frac{d}{dt}\right)\mathbf{\Pi}_m = \frac{n_e e^2}{m_e}\mathbf{E}_m \quad (2.2)$$

Now we introduce optical fields to make use of the rotating wave approximation. From this point onward, complex field envelopes will be represented by purple notation. $\mathbf{\Pi}_m = \frac{1}{2} [\mathbf{\Pi}_m e^{-i\omega t} + \mathbf{\Pi}_m^* e^{i\omega t}]$, $\mathbf{E}_m = \frac{1}{2} [\mathbf{E}_m e^{-i\omega t} + \mathbf{E}_m^* e^{i\omega t}]$. We notice that because of linear independency between $e^{i\omega t}$ and $e^{-i\omega t}$, linear derivatives lead to the following relation for the complex envelope.

$$\frac{d\mathbf{\Pi}_m}{dt} - \frac{\omega^2 + 2i\gamma\omega}{2(\gamma - i\omega)} \mathbf{\Pi}_m = \frac{\varepsilon_0 \omega_{pl}^2}{2(\gamma - i\omega)} \mathbf{E}_m \quad (2.3)$$

ω : frequency of the field;

$\omega_{pl}^2 = \frac{n_e e^2}{m_e \varepsilon_0}$: plasma frequency;

ε_0 : vacuum permittivity.

2.2 The Gain assisted Medium

For a realistic model, we start with the non-linear formula for the polarization of the material, assuming that every dipole moment μ can have a different orientation. The real polarization.

$$\mathbf{\Pi}_h = \frac{n}{4\pi} \int_{4\pi} [\rho_{12} + \rho_{12}^*] \boldsymbol{\mu} d\Omega \quad (2.4)$$

n : volumetric density of atoms; $\boldsymbol{\mu}$: dipole moment;

ρ : defined as the density matrix of the two level system; $\rho_{21} = \rho_{12}^*$.

$$\rho = \begin{bmatrix} \rho_{11} & \rho_{12} \\ \rho_{21} & \rho_{22} \end{bmatrix} \quad (2.5)$$

In this framework, the complex envelope of the polarization of the material is defined as:

$$\frac{1}{2}\mathbf{\Pi}_h = \frac{n}{4\pi} \int_{4\pi} \rho_{12}^* \boldsymbol{\mu} d\Omega \quad (2.6)$$

where the real polarization can be obtained by

$$\mathbf{\Pi}_h = \frac{1}{2} [\mathbf{\Pi}_h + \mathbf{\Pi}_h^*] \quad (2.7)$$

The optical electric field of the host can also be depicted as:

$$\mathbf{E}_h = \frac{1}{2} [\mathbf{E}_h + \mathbf{E}_h^*] \quad (2.8)$$

The two level system in a gain enriched material submerged in a thermal bath is modeled using Optical Bloch equations 6:

$$\frac{d}{dt} \rho_{12}^* + \left(i\omega_{21} + \frac{1}{\tau_2} \right) \rho_{12}^* = -\frac{iN}{\hbar} \boldsymbol{\mu} \cdot \mathbf{E}_h \quad (2.9)$$

$$\frac{dN}{dt} + \frac{N - \tilde{N}}{\tau_1} = \frac{2i}{\hbar} (\rho_{12} - \rho_{12}^*) \boldsymbol{\mu} \cdot \mathbf{E}_h \quad (2.10)$$

$\omega_{21} = \frac{E_2 - E_1}{\hbar}$: transition frequency between levels 1 and 2;

$\tau_2 = \frac{\tau_1}{1 + \tau_1 \gamma_c}$: typical relaxation rate for the phase, also related to the emission

width Δ through $\tau_2 = \frac{2}{\Delta}$;

γ_c : related to the inner collisions coefficient;

τ_1 : the typical relaxation rate for the energy;

N : population inversion $N = \rho_{22} - \rho_{11}$;

\tilde{N} : value of N at equilibrium with the reservoir.

By integrating equation 2.9 over the solid angle, multiplying by $\frac{n}{4\pi}$, and applying a dot product with $\boldsymbol{\mu}$.

$$\frac{d}{dt} \frac{n}{4\pi} \int_{4\pi} \boldsymbol{\rho}_{12}^* \cdot \boldsymbol{\mu} \, d\Omega + \left(i\omega_{12} + \frac{1}{\tau_2} \right) \frac{n}{4\pi} \int_{4\pi} \boldsymbol{\rho}_{12}^* \cdot \boldsymbol{\mu} \, d\Omega = -\frac{iN}{\hbar} \frac{n}{4\pi} \int_{4\pi} (\boldsymbol{\mu} \cdot \mathbf{E}_h) \cdot \boldsymbol{\mu} \, d\Omega \quad (2.11)$$

Using dyadic algebra we can calculate

$$\int_{4\pi} \boldsymbol{\mu} \cdot (\boldsymbol{\mu} \cdot \mathbf{E}_h) \, d\Omega \Rightarrow \int_{4\pi} \mu_i \cdot (\mu_j \cdot \nu_j) \, d\Omega \quad (2.12)$$

$\boldsymbol{\mu} = \mu (\cos \phi \sin \theta, \sin \phi \sin \theta, \cos \theta)$, whence the matrix $\mu_i \mu_j$ is obtained

$$\mu_i \mu_j = \begin{bmatrix} \cos^2 \phi \sin^2 \theta & \sin^2 \theta \sin \phi \cos \theta & \sin \theta \cos \theta \sin \phi \\ \sin \theta \sin \phi \cos \phi & \sin^2 \theta \sin^2 \phi & \sin \theta \sin \phi \cos \phi \\ \sin \theta \cos \phi \sin \phi & \sin \theta \cos \theta \sin \phi & \cos^2 \theta \end{bmatrix} \quad (2.13)$$

terms outside of the diagonal become 0 when integrated over the solid angle. Then

$$\int_{4\pi} \mu_i \cdot (\mu_j \cdot \nu_j) \, d\Omega = \frac{4}{3} \pi \mu^2 \delta_{ij} \nu_j \rightarrow \frac{4}{3} \pi \mu^2 \mathbf{v} \quad (2.14)$$

In this case for $\mathbf{v} = \mathbf{E}_h$.

$$\int_{4\pi} \boldsymbol{\mu} \cdot (\boldsymbol{\mu} \cdot \mathbf{E}_h) \, d\Omega = \frac{4}{3} \pi \mu^2 \mathbf{E}_h \quad (2.15)$$

Using this result in 2.11 the definition in 2.6 is recovered .

$$\frac{d}{dt} \boldsymbol{\Pi}_h + \left(i\omega_{12} + \frac{1}{\tau_2} \right) \frac{n}{4\pi} \boldsymbol{\Pi}_h = -\frac{2inN}{3\hbar} \mu^2 \mathbf{E}_h \quad (2.16)$$

Furthermore, following the same steps, the left side of equation 2.10 becomes

$$\frac{n}{4\pi} \left[\int_{4\pi} \frac{dN}{dt} d\Omega + \int_{4\pi} \frac{N - \tilde{N}}{\tau_1} d\Omega \right] = n \left[\frac{dN}{dt} + \frac{N - \tilde{N}}{\tau_1} \right] \quad (2.17)$$

the right side

$$\frac{2i}{\hbar} \left[\frac{n}{4\pi} \int_{4\pi} \rho_{12} \boldsymbol{\mu} d\Omega - \frac{n}{4\pi} \int_{4\pi} \rho_{12}^* \boldsymbol{\mu} d\Omega \right] \cdot \mathbf{E}_h \quad (2.18)$$

$$\frac{2i}{\hbar} \frac{(\boldsymbol{\Pi}^* - \boldsymbol{\Pi})}{2} \cdot \mathbf{E}_h = \frac{i}{\hbar} (\boldsymbol{\Pi}_h^* - \boldsymbol{\Pi}_h) \cdot \mathbf{E}_h \quad (2.19)$$

and we obtain the system of equations for the time evolution of $\boldsymbol{\Pi}_h$

$$\frac{d}{dt} \boldsymbol{\Pi}_h + \left(i\omega_{12} + \frac{1}{\tau_2} \right) \boldsymbol{\Pi}_h = -\frac{2inN}{3\hbar} \mu^2 \mathbf{E}_h \quad (2.20)$$

$$\frac{dN}{dt} + \frac{N - \tilde{N}}{\tau_1} = -\frac{i}{n\hbar} (\boldsymbol{\Pi}_h - \boldsymbol{\Pi}_h^*) \cdot \mathbf{E}_h \quad (2.21)$$

To solve it, we use solutions of the form.

$$\boldsymbol{\Pi}_h = \frac{1}{2} \left[\boldsymbol{\Pi}_h e^{-i\omega t} + \boldsymbol{\Pi}_h^* e^{i\omega t} \right] \quad (2.22)$$

$$\mathbf{E}_h = \frac{1}{2} \left[\mathbf{E}_h e^{-i\omega t} + \mathbf{E}_h^* e^{i\omega t} \right] \quad (2.23)$$

(abusing notation, the previous $\boldsymbol{\Pi}_h$ becomes $\boldsymbol{\Pi}_h e^{-i\omega t}$).

After derivation 2.20 turns into

$$\frac{d}{dt} \boldsymbol{\Pi}_h - i(\omega - \omega_{12}) \boldsymbol{\Pi}_h + \frac{1}{\tau_2} \boldsymbol{\Pi}_h = -\frac{2inN}{3\hbar} \mu^2 \mathbf{E}_h \quad (2.24)$$

Onto the second OB equation 2.21,

$$-\frac{i}{n\hbar}(\Pi_{\mathbf{h}}e^{-i\omega t} + \Pi_{\mathbf{h}}^*e^{i\omega t}) \cdot \frac{1}{2}\mathbf{E}_{\mathbf{h}}e^{-i\omega t} + \mathbf{E}_{\mathbf{h}}^*e^{i\omega t}) = \quad (2.25)$$

$$-\frac{i}{n\hbar}[\Pi_{\mathbf{h}}\mathbf{E}_{\mathbf{h}}e^{-2i\omega t} + \Pi_{\mathbf{h}}\mathbf{E}_{\mathbf{h}}^* - \Pi_{\mathbf{h}}^*\mathbf{E}_{\mathbf{h}} + \Pi_{\mathbf{h}}^*\mathbf{E}_{\mathbf{h}}e^{-2i\omega t}] \quad (2.26)$$

by averaging over time, terms of the form $e^{-2i\omega t}$ become negligible. Equation 2.21 is then

$$\frac{dN}{dt} + \frac{N - \tilde{N}}{\tau_1} = -\frac{i}{2n\hbar}(\Pi_{\mathbf{h}}\mathbf{E}_{\mathbf{h}}^* - \Pi_{\mathbf{h}}^*\mathbf{E}_{\mathbf{h}}) \quad (2.27)$$

2.2.1 Normalization

It is easier to deal with a normalized system of equation found with the following normalized variables:

$$\hat{t} = \omega_{pl}t, \quad \hat{\omega} = \frac{\omega}{\omega_{pl}} \quad (2.28)$$

$$\hat{r} = \frac{r}{a}, \quad \hat{n} = a^3n \quad (2.29)$$

$$\hat{E} = \sqrt{\frac{\varepsilon_0}{n\hbar\omega_{pl}}}E \quad (2.30)$$

$$\hat{P} = \frac{P}{\sqrt{\varepsilon_0 n\hbar\omega_{pl}}} \quad (2.31)$$

n: Gain elements molecular density; \hbar : reduced Planck constant

Consequently

$$\hat{\mu}^2 = \frac{2\mu^2}{3\varepsilon_0 n\hbar\omega_{pl}a^6} \quad (2.32)$$

Introducing all of these variables in equations 2.24, 2.27, 2.3 leads to

$$\frac{d}{dt}\mathbf{\Pi}_h - \left[i(\omega - \omega_{12}) - \frac{1}{\tau_2} \right] \mathbf{\Pi}_h = -in^2\mu^2\mathbf{E}_h \quad (2.33)$$

$$\frac{dN}{dt} + \frac{N - \tilde{N}}{\tau_1} = -\frac{i}{2}(\mathbf{\Pi}_h\mathbf{E}_h^* - \mathbf{\Pi}_h^*\mathbf{E}_h) \quad (2.34)$$

2.3 Steady state permittivity

During linear amplification the left side of 2.34 is negligible and N converges rapidly ($N \rightarrow \tilde{N}$).

The condition for finding the steady state is $\frac{dN}{dt} = 0$, and using the relation $\frac{1}{\tau_2} = \frac{\Delta}{2}$ in 2.33 gives

$$\mathbf{\Pi}_h = \frac{2n^2\mu^2\tilde{N}}{2(\omega - \omega_{12}) + i\Delta}\mathbf{E}_h \quad (2.35)$$

The polarization and the electric field are linked through:

$$\mathbf{\Pi}_h = \chi(\omega)\mathbf{E}_h \quad (2.36)$$

where $\chi(\omega)$ is the complex normalized susceptibility.

$$\chi(\omega) = \frac{2n^2\mu^2\tilde{N}}{2(\omega - \omega_{12}) + i\Delta} \quad (2.37)$$

susceptibility in the transition frequency $\chi(\omega_{21})$ is calculated

$$\chi(\omega_{21}) = -\frac{i2n^2\mu^2\tilde{N}}{\Delta} \quad (2.38)$$

And the positive parameter accounting for the quantity of gain in the system G is found as $\chi(\omega_{21}) = -iG$.

$$G = n^2 \mu^2 \tilde{N} \tau_2 \quad (2.39)$$

susceptibility becomes

$$\chi(\omega) = \frac{G\Delta}{2(\omega - \omega_{12}) + i\Delta} \quad (2.40)$$

Moving on, the total polarization in the metal has to take into account the polarization of the ionic lattice.

$$\mathbf{P}_m = \chi_b \mathbf{E}_m + \mathbf{\Pi}_m \quad (2.41)$$

and the polarization of the host is obtained by averaging the dipole moments of the gain elements assuming that they are oriented randomly with respect to E_h , as was derived in A.2

$$\mathbf{P}_h = \varepsilon_0 \chi_b \mathbf{E}_h + \frac{n}{4\pi} \int_{4\pi} (\rho_{12} + \rho_{21}) \mu \, d\Omega \quad (2.42)$$

using definition 2.6 in 2.42 gives

$$\mathbf{P}_h = \varepsilon_0 \chi_b \mathbf{E}_h + \Re[\mathbf{\Pi}_h] \quad (2.43)$$

Subsequently, the rotating wave approximation can be used to find the time evolution of the complex envelopes.

$$\mathbf{P}_h = \varepsilon_0 \chi_b \mathbf{E}_h + \mathbf{\Pi}_h \quad (2.44)$$

Ultimately, the full system of equations that describe the time evolution of both the polarizability and the electromagnetic fields is:

$$\frac{d}{dt}\mathbf{\Pi}_h - \left[i(\omega - \omega_{12}) - \frac{1}{\tau_2} \right] \mathbf{\Pi}_h = -\frac{iG}{\tau_2} \frac{N}{\tilde{N}} \mathbf{E}_h \quad (2.45)$$

$$\frac{dN}{dt} + \frac{N - \tilde{N}}{\tau_1} = -\frac{i}{2} (\mathbf{\Pi}_h \mathbf{E}_h^* - \mathbf{\Pi}_h^* \mathbf{E}_h) \quad (2.46)$$

$$\frac{d\mathbf{\Pi}_m}{dt} - \frac{\omega^2 + 2i\gamma\omega}{2(\gamma - i\omega)} \mathbf{\Pi}_m = \frac{1}{2(\gamma - i\omega)} \mathbf{E}_m \quad (2.47)$$

$$\mathbf{P}_h = \varepsilon_0 \chi_b \mathbf{E}_h + \mathbf{\Pi}_h(t) \quad (2.48)$$

$$\mathbf{P}_m = \chi_b \mathbf{E}_m + \mathbf{\Pi}_m(t) \quad (2.49)$$

ε_0 : vacuum permittivity;

χ_∞ : susceptibility due to the metal ions;

χ_b : susceptibility of the dielectric in which the gain elements are dissolved;

E_h, E_m : gain medium and metal electric fields correspondingly.

Polarization can then be divided in a constant term and a dynamic polarization that will be fully modelled in the next section.

Chapter 3

Mie Theory

The model we developed aims to predict the behaviour of particles of any size, not only in the quasi-static limit. For this end, we use vector spherical harmonics to project the electric fields as it is done in Mie theory [64].

The vector spherical harmonics are complex valued functions expressed in spherical coordinates, and can be found as an extension of scalar spherical harmonics, as follows.

$$\mathbf{M}_{\text{enm}} = \nabla \times [\mathbf{R}\psi_{emn}] \quad (3.1)$$

$$\mathbf{M}_{\text{onm}} = \nabla \times [\mathbf{R}\psi_{omn}] \quad (3.2)$$

$$\mathbf{N}_{\text{enm}} = \frac{\nabla \times \mathbf{M}_{\text{emn}}}{k} \quad (3.3)$$

$$\mathbf{N}_{\text{onm}} = \frac{\nabla \times \mathbf{M}_{\text{omn}}}{k} \quad (3.4)$$

$\psi(R)$ is a generating function that obeys the scalar Helmholtz equation.

$$\nabla^2\psi(\mathbf{R}) - k^2\psi(\mathbf{R}) = 0 \quad (3.5)$$

Two linearly independent solutions, odd and even, can be found in this manner for 3.5. Namely

$$\psi_{emn}(\mathbf{R}) = \cos(m\Phi)P_n^m(\cos\theta)z_n(kR) \quad (3.6)$$

$$\psi_{omn}(\mathbf{R}) = \sin(m\Phi)P_n^m(\cos\theta)z_n(kR) \quad (3.7)$$

z_n : Bessel functions corresponding to the radial coordinate kR ;

$P_n^m(\cos\theta)$: associated Legendre polynomials.

Since ψ_{emn} and ψ_{omn} produce a complete base, any solution to the Helmholtz equation can be written as a linear combination of them.

After lengthy algebra the spherical harmonics can be written as:

$$\mathbf{M}_{\mathbf{enm}} = -\sin\phi\pi_n(\theta)z_n(\rho)\hat{\theta}(\theta,\phi) - \cos\phi\tau_n(\theta)z_n(\rho)\hat{\phi}(\phi) \quad (3.8)$$

$$\mathbf{M}_{\mathbf{onm}} = \cos\phi\pi_n(\theta)z_n(\rho)\hat{\theta}(\theta,\phi) - \sin\phi\tau_n(\theta)z_n(\rho)\hat{\phi}(\phi) \quad (3.9)$$

$$\begin{aligned} \mathbf{N}_{\mathbf{onm}} = & n(n+1)\sin\phi\sin\theta\pi_n(\theta)\frac{z_n(\rho)}{\rho}\hat{R}(\theta,\phi) \\ & + \sin\phi\tau_n(\theta)\frac{[\rho z_n(\rho)]'}{\rho}\hat{\theta}(\theta,\phi) + \cos\phi\pi_n(\theta)\frac{[\rho z_n(\rho)]'}{\rho}\hat{\phi}(\phi) \end{aligned} \quad (3.10)$$

$$\begin{aligned} \mathbf{N}_{\text{enm}} = & n(n+1) \cos \phi \sin \theta \pi_n(\theta) \frac{z_n(\rho)}{\rho} \hat{R}(\theta, \phi) \\ & + \cos \phi \tau_n(\theta) \frac{[\rho z_n(\rho)]'}{\rho} \hat{\theta}(\theta, \phi) - \sin \phi \pi_n(\theta) \frac{[\rho z_n(\rho)]'}{\rho} \hat{\phi}(\phi) \end{aligned} \quad (3.11)$$

π_n, τ_n : angular dependency functions:

$$\begin{aligned} \pi_n(\theta) &= \frac{P_n^1(\cos \theta)}{\sin \theta}, \\ \tau_n(\theta) &= \frac{dP_n^1(\cos \theta)}{d\theta}; \end{aligned}$$

$\rho = kR$: radial variable; k : related to the relative refraction index between the media; R : modulus of distance from the origin.

Ultimately, we can express any field that obeys the Helmholtz equation with its vector spherical harmonics representation.

$$\mathbf{E}_\alpha = \sum_{n,m}^{\infty} \left[\mathbf{B}_{\text{emn}} \mathbf{M}_{\text{emn}} + \mathbf{B}_{\text{omn}} \mathbf{M}_{\text{omn}} + \mathbf{A}_{\text{emn}} \mathbf{N}_{\text{emn}} + \mathbf{A}_{\text{omn}} \mathbf{N}_{\text{omn}} \right] \quad (3.12)$$

where each of the coefficients $A_{\mu,\nu,\lambda}$ and $B_{\mu,\nu,\lambda}$ are calculated by projecting the given field over the spherical harmonics and using the orthogonality of the associated Legendre polynomials.

With these mathematical tools and after extensive algebra, the spherical harmonics representation of a plane wave travelling in the \hat{z} direction $\mathbf{E}_i = \mathbf{E}_0 e^{ikz} \hat{i}$ is found to be [64]

$$\mathbf{E}_{\text{inc}}(\mathbf{r}, t) = \sum_{n=1}^{\infty} \mathbf{E}_n \left[\mathbf{M}_{\mathbf{o}1n}^{(1)}(\mathbf{r}) - i \mathbf{N}_{\mathbf{e}1n}^{(1)}(\mathbf{r}) \right] \quad (3.13)$$

Each mode n characterizes a different mode in the multipole expansion. Taking into account that divergences at the origin must be avoided, the incident \mathbf{E}_{in} and scattered fields \mathbf{E}_{sca} .

$$\mathbf{E}_{\text{in}}(\mathbf{r}, t) = \sum_{n=1}^{\infty} \mathbf{E}_n \left[c_n \mathbf{M}_{\text{oln}}^{(1)}(\mathbf{r}) - i d_n \mathbf{N}_{\text{eln}}^{(1)}(\mathbf{r}) \right] \quad (3.14)$$

$$\mathbf{E}_{\text{sca}}(\mathbf{r}, t) = \sum_{n=1}^{\infty} \mathbf{E}_n \left[i a_n \mathbf{N}_{\text{eln}}^{(3)}(\mathbf{r}) - b_n \mathbf{M}_{\text{oln}}^{(3)}(\mathbf{r}) \right] \quad (3.15)$$

$$E_n = i^n \frac{2n+1}{n(n+1)} E_0$$

E_0 : amplitude of the incident field;

superindex ⁽¹⁾: $z_n(\rho) = j_n(\rho)$ to avoid a singularity at the origin;

superindex ⁽³⁾: $z_n(\rho) = h_n^{(1)}(\rho)$.

By the superposition principle the electric field of the gain medium is the sum of \mathbf{E}_{inc} and \mathbf{E}_{sca} , and the electric field inside the metal is simply \mathbf{E}_{in} . We also define $\tilde{a}_n = E_0 a_n$, $\tilde{b}_n = E_0 b_n$, $\tilde{c}_n = E_0 c_n$, and $\tilde{d}_n = E_0 d_n$.

$$\mathbf{E}_{\text{m}} = \sum_{n=1}^{\infty} i^n \frac{2n+1}{n(n+1)} \left[\tilde{c}_n \mathbf{M}_{\text{oln}}^{(1)}(\mathbf{r}) - i \tilde{d}_n \mathbf{N}_{\text{eln}}^{(1)}(\mathbf{r}) \right] \quad (3.16)$$

$$\mathbf{E}_{\text{h}} = \sum_{n=1}^{\infty} i^n \frac{2n+1}{n(n+1)} \left\{ \mathbf{E}_0 \left[\mathbf{M}_{\text{oln}}^{(1)}(\mathbf{r}) - i \mathbf{N}_{\text{eln}}^{(1)}(\mathbf{r}) \right] + i \tilde{a}_n \mathbf{N}_{\text{eln}}^{(3)}(\mathbf{r}) - \tilde{b}_n \mathbf{M}_{\text{oln}}^{(3)}(\mathbf{r}) \right\} \quad (3.17)$$

We assume a similar shape for the dynamical part of the polarizations

$$\mathbf{\Pi}_{\text{m}} = \sum_{n=1}^{\infty} i^n \frac{2n+1}{n(n+1)} \left[\kappa_n \mathbf{M}_{\text{oln}}^{(1)}(\mathbf{r}) - i \delta_n \mathbf{N}_{\text{eln}}^{(1)}(\mathbf{r}) \right] \quad (3.18)$$

$$\mathbf{\Pi}_h = \sum_{n=1}^{\infty} i^n \frac{2n+1}{n(n+1)} \left[\zeta_n \mathbf{M}_{\mathbf{e}1n}^{(1)}(\mathbf{r}) - i\eta_n \mathbf{N}_{\mathbf{e}1n}^{(1)}(\mathbf{r}) + i\alpha_n \mathbf{N}_{\mathbf{e}1n}^{(3)}(\mathbf{r}) - \beta_n \mathbf{M}_{\mathbf{e}1n}^{(3)}(\mathbf{r}) \right] \quad (3.19)$$

By using Maxwell's third equation for oscillating fields $\nabla \times \mathbf{E}_\alpha = i\omega\mu\mathbf{E}_\alpha$ the magnetic fields of the metal and host can be written as:

$$\mathbf{H}_m = -\frac{k_1}{\omega\mu_1} \sum_{n=1}^{\infty} i^n \frac{2n+1}{n(n+1)} \left[\tilde{d}_n \mathbf{M}_{\mathbf{e}1n}^{(1)}(\mathbf{r}) + i\tilde{c}_n \mathbf{N}_{\mathbf{e}1n}^{(1)}(\mathbf{r}) \right] \quad (3.20)$$

$$\mathbf{H}_h = -\frac{k}{\omega\mu} \sum_{n=1}^{\infty} i^n \frac{2n+1}{n(n+1)} \left\{ \mathbf{E}_0 \left[\mathbf{M}_{\mathbf{e}1n}^{(1)}(\mathbf{r}) + i\mathbf{N}_{\mathbf{e}1n}^{(1)}(\mathbf{r}) \right] - i\tilde{b}_n \mathbf{N}_{\mathbf{e}1n}^{(3)}(\mathbf{r}) - \tilde{a}_n \mathbf{M}_{\mathbf{e}1n}^{(3)}(\mathbf{r}) \right\} \quad (3.21)$$

At last, plugging in the Mie expansion of the fields into the system of equations 2.3 - 2.33, one obtains a new system of equations for the time evolution of the coefficients.

For easier handling of the equations we define constants.

$$\tilde{G} = -\frac{iGN}{\tau_2 \tilde{N}}; \quad \Omega_H = \left[i(\omega - \omega_{12}) - \frac{1}{\tau_2} \right]; \quad (3.22)$$

$$\Omega_p = \frac{\omega^2 + 2i\gamma\omega}{2(\gamma - i\omega)}; \quad \Gamma_p = \frac{1}{2(\gamma - i\omega)} \quad (3.23)$$

$$\frac{d}{dt} \alpha_n - \Omega_h \alpha_n = \tilde{G} \tilde{a}_n \quad (3.24)$$

$$\frac{d}{dt} \beta_n - \Omega_h \beta_n = \tilde{G} \tilde{b}_n \quad (3.25)$$

$$\frac{d}{dt}\kappa_n - \Omega_p\kappa_n = \Gamma_p c_n \quad (3.26)$$

$$\frac{d}{dt}\delta_n - \Omega_p\delta_n = \Gamma_p d_n \quad (3.27)$$

$$\frac{d}{dt}\eta_n - \Omega_h\eta_n = \tilde{G}E_0 \quad (3.28)$$

$$\frac{d}{dt}\zeta_n - \Omega_h\zeta_n = \tilde{G}E_0 \quad (3.29)$$

Time evolution of the coefficients determines the evolution of the electric fields.

3.1 Boundary conditions

In order to preserve tangential continuity on the surface of the nanosphere when $r = a$, these conditions must hold. $\mathbf{\Pi}_T$ is the total polarization.

$$(\mathbf{E}_h - \mathbf{E}_m) \times \hat{R}(\theta, \phi) = 0 \quad (3.30)$$

$$(\mathbf{H}_m - \mathbf{H}_h) \cdot \hat{\phi}(\phi) = \frac{d\mathbf{\Pi}_T}{dt}(\hat{\theta}(\theta, \phi) \times \hat{R}(\theta, \phi)) \quad (3.31)$$

$$(\mathbf{H}_m - \mathbf{H}_h) \cdot \hat{\theta}(\theta, \phi) = \frac{d\mathbf{\Pi}_T}{dt}(\hat{\phi}(\phi) \times \hat{R}(\theta, \phi)) \quad (3.32)$$

3.1.1 Tangential continuity Electric Field

We note that the parameter $\rho = kR$ on the surface of the metal becomes $\rho = k_1 a = mx$ and in the gain medium $\rho = ka = x$.

Condition 3.30 becomes:

$$\mathbf{E}_m^\theta(a\hat{R}(\theta, \phi)) \Big|_{\rho=mx} = \mathbf{E}_n^\theta(a\hat{R}(\theta, \phi)) \Big|_{\rho=x} \quad (3.33)$$

$$\mathbf{E}_m^\phi(a\hat{R}(\theta, \phi)) \Big|_{\rho=mx} = \mathbf{E}_n^\phi(a\hat{R}(\theta, \phi)) \Big|_{\rho=x} \quad (3.34)$$

From 3.33, plugging in 3.16, 3.17.

$$\begin{aligned} & \left[\tilde{c}_n \mathbf{M}_{\mathbf{o}1\mathbf{n}}^{(1)} - i\tilde{d}_n \mathbf{N}_{\mathbf{e}1\mathbf{n}}^{(1)} \right] \Big|_{\rho=mx}^\theta \\ &= \left[\mathbf{E}_0 \mathbf{M}_{\mathbf{o}1\mathbf{n}}^{(1)} - i\mathbf{E}_0 \mathbf{N}_{\mathbf{e}1\mathbf{n}}^{(1)} + i\tilde{a}_n \mathbf{N}_{\mathbf{e}1\mathbf{n}}^{(3)} - i\tilde{d}_n \mathbf{M}_{\mathbf{o}1\mathbf{n}}^{(3)} \right] \Big|_{\rho=x}^\theta \end{aligned} \quad (3.35)$$

expanding theta components of VSH defined in 3.8 - 3.11 we get.

$$\begin{aligned} & \mathbf{E}_0 \cos \phi \pi_n(\theta) j_n(x) - i\mathbf{E}_0 \cos \phi \tau_n(\theta) \frac{[x j_n(x)]'}{x} + i\tilde{a}_n \cos \phi \tau_n(\theta) \frac{[x h_n^{(1)}(x)]'}{x} - \tilde{b}_n \cos \phi \pi_n(\theta) h_n^{(1)}(x) \\ &= \tilde{c}_n \cos \phi \pi_n(\theta) j_n(mx) - i\tilde{d}_n \cos \phi \tau_n(\theta) \frac{[mx j_n(mx)]'}{mx} \end{aligned} \quad (3.36)$$

which can be reorganized as:

$$\begin{aligned} & \pi_n(\theta) \left[\tilde{c}_n j_n(mx) - \mathbf{E}_0 j_n(x) + \tilde{b}_n h_n^{(1)}(x) \right] = \\ & i\tau_n(\theta) \left\{ \tilde{d}_n \frac{[mx j_n(mx)]'}{mx} - \mathbf{E}_0 \frac{[x j_n(x)]'}{x} + \tilde{a}_n \frac{[x h_n^{(1)}(x)]'}{x} \right\} \end{aligned} \quad (3.37)$$

Repeating the same process on condition 3.34 yields:

$$\begin{aligned}
& -\tilde{c}_n \sin \phi \tau_n(\theta) j_n(mx) + i \tilde{d}_n \sin \phi \pi_n(\theta) \frac{[mx j_n(mx)]'}{mx} = \\
& -\mathbf{E}_0 \sin \phi \tau_n(\theta) j_n(x) + i \mathbf{E}_0 \sin \phi \pi_n(\theta) \frac{[x j_n(x)]'}{x} \\
& -i \tilde{a}_n \sin \phi \pi(\theta) \frac{[x h_n^{(1)}(x)]'}{x} + \tilde{b}_n \sin \phi \tau_n(\theta) h_n^{(1)}(x) \quad (3.38)
\end{aligned}$$

which can be reorganized as:

$$\begin{aligned}
\tau_n(\theta) \left[\tilde{c}_n j_n(mx) - \mathbf{E}_0 j_n(x) + \tilde{b}_n h_n^{(1)}(x) \right] = \\
i \pi_n(\theta) \left\{ \tilde{d}_n \frac{[mx j_n(mx)]'}{mx} - \mathbf{E}_0 \frac{[x j_n(x)]'}{x} + \tilde{a}_n \frac{[x h_n^{(1)}(x)]'}{x} \right\} \quad (3.39)
\end{aligned}$$

for a more straightforward handling of the equations, we define

$$\boxed{\square} = \left[\tilde{c}_n j_n(mx) - \mathbf{E}_0 j_n(x) + \tilde{b}_n h_n^{(1)}(x) \right] \quad (3.40)$$

$$\boxed{\boxtimes} = \left\{ \tilde{d}_n \frac{[mx j_n(mx)]'}{mx} - \mathbf{E}_0 \frac{[x j_n(x)]'}{x} + \tilde{a}_n \frac{[x h_n^{(1)}(x)]'}{x} \right\} \quad (3.41)$$

summing 3.37 with 3.39 we get

$$\left(\pi_n(\theta) + \tau_n(\theta) \right) \boxed{\square} = i \left(\pi_n(\theta) + \tau_n(\theta) \right) \boxed{\boxtimes} \quad (3.42)$$

subtracting 3.37 from 3.39 we get

$$\left(\pi_n(\theta) - \tau_n(\theta) \right) \boxed{\square} = -i \left(\pi_n(\theta) - \tau_n(\theta) \right) \boxed{\boxtimes} \quad (3.43)$$

Then necessarily \boxtimes and \boxminus must independently be zero. Besides, since $\pi_n + \tau_n$ and $\pi_n - \tau_n$ are orthogonal, this is verified independently for every n . We arrive at two more conditions.

$$j_n(mx)\tilde{c}_n + h_n^{(1)}(x)\tilde{b}_n = j_n(x)\mathbf{E}_0 \quad (3.44)$$

$$[mxj_n(mx)]'\tilde{d}_n + m[xh_n^{(1)}(x)]'\tilde{a}_n = m[xj_n(x)]'\mathbf{E}_0 \quad (3.45)$$

3.1.2 Tangential continuity Magnetic Field

Conditions 3.31 , 3.32 lead to:

$$\mathbf{H}_m^\theta(a\hat{R}(\theta, \phi))\Big|_{\rho=mx} - \mathbf{H}_h^\theta(a\hat{R}(\theta, \phi))\Big|_{\rho=x} = -\frac{d}{dt}\mathbf{H}_m^\phi(a\hat{R}(\theta, \phi))\Big|_{\rho=mx} - \frac{d}{dt}\mathbf{H}_h^\phi(a\hat{R}(\theta, \phi))\Big|_{\rho=x} \quad (3.46)$$

$$\mathbf{H}_m^\phi(a\hat{R}(\theta, \phi))\Big|_{\rho=mx} - \mathbf{H}_h^\phi(a\hat{R}(\theta, \phi))\Big|_{\rho=x} = \frac{d}{dt}\mathbf{H}_m^\theta(a\hat{R}(\theta, \phi))\Big|_{\rho=mx} + \frac{d}{dt}\mathbf{H}_h^\theta(a\hat{R}(\theta, \phi))\Big|_{\rho=x} \quad (3.47)$$

employing 3.46.

$$\begin{aligned} & -\frac{k_1}{\omega\mu_1} \left[\tilde{d}_n \mathbf{M}_{e1n}^{(1)} + i\tilde{c}_n \mathbf{N}_{o1n}^{(1)} \right] \Big|_{\rho=mx}^\theta + \frac{k}{\omega\mu} \left\{ \mathbf{E}_0 [\mathbf{M}_{e1n}^{(1)} + i\mathbf{N}_{o1n}^{(1)}] + i\tilde{b}_n \mathbf{M}_{e1n}^{(3)} + \tilde{a}_n \mathbf{N}_{o1n}^{(3)} \right\} \Big|_{\rho=x}^\theta \\ & = -\frac{d}{dt} \left[\kappa_n \mathbf{M}_{o1n}^{(1)} - i\delta_n \mathbf{N}_{e1n}^{(1)} \right] \Big|_{\rho=mx}^\phi \\ & - \frac{d}{dt} \left[\zeta_n \mathbf{M}_{o1n}^{(1)} - i\eta_n \mathbf{N}_{e1n}^{(1)} + i\alpha_n \mathbf{N}_{e1n}^{(3)} - \beta_n \mathbf{M}_{o1n}^{(3)} \right] \Big|_{\rho=x}^\phi \quad (3.48) \end{aligned}$$

In a similar manner to last section.

$$\begin{aligned}
\pi_n(\theta) & \left[-j_n(x) \mathbf{E}_0 + mj_n(mx) \tilde{d}_n + h_n^{(1)}(x) \tilde{a}_n \right. \\
& \left. + \frac{i\omega}{k} \frac{[mxj_n(mx)]'}{mx} \frac{d\delta_n}{dt} + \frac{i\omega}{k} \frac{[xh_n^{(1)}(x)]'}{x} \frac{d\alpha_n}{dt} - \frac{i\omega}{k} \frac{[xj_n(x)]'}{x} \frac{d\eta_n}{dt} \right] = \\
& i\tau_n(\theta) \left\{ \frac{[xj_n(x)]'}{x} \mathbf{E}_0 - m \frac{[mxj_n(mx)]'}{mx} \tilde{c}_n - \frac{[xh_n^{(1)}(x)]'}{x} \tilde{b}_n \right. \\
& \left. + \frac{i\omega}{k} j_n(x) \frac{d\zeta_n}{dt} + \frac{i\omega}{k} j_n(mx) \frac{d\kappa_n}{dt} - \frac{i\omega}{k} h_n(x) \frac{d\beta_n}{dt} \right\} \quad (3.49)
\end{aligned}$$

likewise, using 3.47

$$\begin{aligned}
& -\frac{k_1}{\omega\mu_1} \left[\tilde{d}_n \mathbf{M}_{e1n}^{(1)} + i\tilde{c}_n \mathbf{N}_{o1n}^{(1)} \right] \Big|_{\rho=mx}^{\phi} + \frac{k}{\omega\mu} \left\{ \mathbf{E}_0 [\mathbf{M}_{e1n}^{(1)} + i\mathbf{N}_{o1n}^{(1)}] + i\tilde{b}_n \mathbf{M}_{e1n}^{(3)} + \tilde{a}_n \mathbf{N}_{o1n}^{(3)} \right\} \Big|_{\rho=x}^{\phi} \\
& = \frac{d}{dt} \left[\kappa_n \mathbf{M}_{o1n}^{(1)} - i\delta_n \mathbf{N}_{e1n}^{(1)} \right] \Big|_{\rho=mx}^{\theta} \\
& + \frac{d}{dt} \left[\zeta_n \mathbf{M}_{o1n}^{(1)} - i\eta_n \mathbf{N}_{e1n}^{(1)} + i\alpha_n \mathbf{N}_{e1n}^{(3)} - \beta_n \mathbf{M}_{o1n}^{(3)} \right] \Big|_{\rho=x}^{\theta} \quad (3.50)
\end{aligned}$$

expanding the expression in VSH:

$$\begin{aligned}
i\pi_n(\theta) & \left[-j_n(x) \mathbf{E}_0 + mj_n(mx) \tilde{d}_n + h_n^{(1)}(x) \tilde{a}_n \right. \\
& \left. + \frac{i\omega}{k} \frac{[mxj_n(mx)]'}{mx} \frac{d\delta_n}{dt} + \frac{i\omega}{k} \frac{[xh_n^{(1)}(x)]'}{x} \frac{d\alpha_n}{dt} - \frac{i\omega}{k} \frac{[xj_n(x)]'}{x} \frac{d\eta_n}{dt} \right] = \\
& \tau_n(\theta) \left\{ \frac{[xj_n(x)]'}{x} \mathbf{E}_0 - m \frac{[mxj_n(mx)]'}{mx} \tilde{c}_n - \frac{[xh_n^{(1)}(x)]'}{x} \tilde{b}_n \right. \\
& \left. + \frac{i\omega}{k} j_n(x) \frac{d\zeta_n}{dt} + \frac{i\omega}{k} j_n(mx) \frac{d\kappa_n}{dt} - \frac{i\omega}{k} h_n(x) \frac{d\beta_n}{dt} \right\} \quad (3.51)
\end{aligned}$$

which leads to the final two conditions.

$$\frac{i\omega}{k} \frac{[mxj_n(mx)]'}{mx} \frac{d\delta_n}{dt} + \frac{i\omega}{k} \frac{[xh_n^{(1)}(x)]'}{x} \frac{d\alpha_n}{dt} - \frac{i\omega}{k} \frac{[xj_n(x)]'}{x} \frac{d\eta_n}{dt} = j_n(x)\mathbf{E}_0 - mj_n(mx)\tilde{d}_n - h_n^{(1)}(x)\tilde{a}_n \quad (3.52)$$

$$m \frac{[mxj_n(mx)]'}{mx} \tilde{c}_n + \frac{[xh_n^{(1)}(x)]'}{x} \tilde{b}_n - \frac{[xj_n(x)]'}{x} \mathbf{E}_0 = \frac{i\omega}{k} j_n(x) \frac{d\zeta_n}{dt} + \frac{i\omega}{k} j_n(mx) \frac{d\kappa_n}{dt} - \frac{i\omega}{k} h_n(x) \frac{d\beta_n}{dt} \quad (3.53)$$

3.2 Time evolution of coefficients

The four conditions that relate the coefficients of the fields are.

$$j_n(mx)\tilde{c}_n + h_n^{(1)}(x)\tilde{b}_n = j_n(x)\mathbf{E}_0 \quad (3.54)$$

$$[mxj_n(mx)]'\tilde{d}_n + m[xh_n^{(1)}(x)]'\tilde{a}_n = m[xj_n(x)]'\mathbf{E}_0 \quad (3.55)$$

$$\frac{i\omega}{k} \frac{[mxj_n(mx)]'}{mx} \frac{d\delta_n}{dt} + \frac{i\omega}{k} \frac{[xh_n^{(1)}(x)]'}{x} \frac{d\alpha_n}{dt} - \frac{i\omega}{k} \frac{[xj_n(x)]'}{x} \frac{d\eta_n}{dt} = j_n(x)\mathbf{E}_0 - mj_n(mx)\tilde{d}_n - h_n^{(1)}(x)\tilde{a}_n \quad (3.56)$$

$$m \frac{[mxj_n(mx)]'}{mx} \tilde{c}_n + \frac{[xh_n^{(1)}(x)]'}{x} \tilde{b}_n - \frac{[xj_n(x)]'}{x} \mathbf{E}_0 = \frac{i\omega}{k} j_n(x) \frac{d\zeta_n}{dt} + \frac{i\omega}{k} j_n(mx) \frac{d\kappa_n}{dt} - \frac{i\omega}{k} h_n(x) \frac{d\beta_n}{dt} \quad (3.57)$$

We identify the time derivatives of the coefficients in conditions 3.56 and 3.57. Together with 3.24 - 3.27 it is a coupled system of equations for the time evolution of the coefficients that can be most effectively represented by matrices. We define the coefficients vector

$$\mathbf{q} = \left\{ \alpha_n, \beta_n, \kappa_n, \delta_n, \eta_n, \zeta_n, \mathbf{E}_0 \right\} \quad (3.58)$$

The system is solved by considering that by choosing the right coefficients p_{ij} , \tilde{a}_n can be found as a function of \tilde{d}_n , \tilde{b}_n as a function of \tilde{c}_n , and vice-versa.

$$\tilde{a}_n = p_{00}q_0 + p_{01}q_1 + p_{02}q_2 + p_{03}q_3 + p_{04}q_4 + p_{05}q_5 + p_{06}q_6 \quad (3.59)$$

$$\tilde{b}_n = p_{10}q_0 + p_{11}q_1 + p_{12}q_2 + p_{13}q_3 + p_{14}q_4 + p_{15}q_5 + p_{16}q_6 \quad (3.60)$$

$$\tilde{c}_n = p_{20}q_0 + p_{21}q_1 + p_{22}q_2 + p_{23}q_3 + p_{24}q_4 + p_{25}q_5 + p_{26}q_6 \quad (3.61)$$

$$\tilde{d}_n = p_{30}q_0 + p_{31}q_1 + p_{32}q_2 + p_{33}q_3 + p_{34}q_4 + p_{35}q_5 + p_{36}q_6 \quad (3.62)$$

Finally, plugging the relations onto system of equations 3.24 - 3.27 gives.

$$\frac{d}{dt}q_0 = (\Omega_h + \tilde{G}p_{00})q_0 + \tilde{G}p_{01}q_1 + \tilde{G}p_{02}q_2 + \tilde{G}p_{03}q_3 + \tilde{G}p_{04}q_4 + \tilde{G}p_{05}q_5 + \tilde{G}p_{06}q_6 \quad (3.63)$$

$$\frac{d}{dt}q_1 = \tilde{G}p_{10}q_0 + (\Omega_h + \tilde{G}p_{11})q_1 + \tilde{G}p_{12}q_2 + \tilde{G}p_{13}q_3 + \tilde{G}p_{14}q_4 + \tilde{G}p_{15}q_5 + \tilde{G}p_{16}q_6 \quad (3.64)$$

$$\frac{d}{dt}q_2 = \Gamma_p p_{20}q_0 + \Gamma_p p_{21}q_1 + (\Omega_p + \Gamma_p p_{22})q_2 + \Gamma_p p_{23}q_3 + \Gamma_p p_{24}q_4 + \Gamma_p p_{25}q_5 + \Gamma_p p_{26}q_6 \quad (3.65)$$

$$\frac{d}{dt}q_3 = \Gamma_p p_{30}q_0 + \Gamma_p p_{31}q_1 + \Gamma_p p_{32}q_2 + (\Omega_p + \Gamma_p p_{33})q_3 + \Gamma_p p_{34}q_4 + \Gamma_p p_{35}q_5 + \Gamma_p p_{36}q_6 \quad (3.66)$$

$$\frac{d}{dt}q_4 = \Omega_h q_4 + \tilde{G}q_6 \quad (3.67)$$

$$\frac{d}{dt}q_5 = \Omega_h q_5 + \tilde{G}q_6 \quad (3.68)$$

Which becomes.

$$p = \begin{pmatrix} (\Omega_h + \tilde{G}p_{00}) & \tilde{G}p_{01} & \tilde{G}p_{02} & \tilde{G}p_{03} & \tilde{G}p_{04} & \tilde{G}p_{05} \\ \tilde{G}p_{10} & (\Omega_h + \tilde{G}p_{11}) & \tilde{G}p_{12} & \tilde{G}p_{13} & \tilde{G}p_{14} & \tilde{G}p_{15} \\ \Gamma_p p_{20} & \Gamma_p p_{21} & (\Omega_p + \Gamma_p p_{22}) & \Gamma_p p_{23} & \Gamma_p p_{24} & \Gamma_p p_{25} \\ \Gamma_p p_{30} & \Gamma_p p_{31} & \Gamma_p p_{32} & (\Omega_p + \Gamma_p p_{33}) & \Gamma_p p_{34} & \Gamma_p p_{35} \\ 0 & 0 & 0 & 0 & \Omega_h & 0 \\ 0 & 0 & 0 & 0 & 0 & \Omega_h \end{pmatrix} \quad (3.69)$$

and the vector for the inhomogenous solution, taking into account that $\mathbf{q}_6 = \mathbf{E}_0$.

$$B = \mathbf{E}_0 \left\{ \tilde{G}p_{06}, \tilde{G}p_{16}, \Gamma_p p_{26}, \Gamma_p p_{36}, \tilde{G}, \tilde{G} \right\} \quad (3.70)$$

It is noticeable that following our definition of $\tilde{a}_n, \tilde{b}_n, \tilde{c}_n, \tilde{d}_n$, dependence on the incident field E_0 is explicit only in the inhomogenous solution of the system.

At long last, the solution to the time evolution of the coefficients can numerically be found in the form:

$$\frac{d}{dt}\mathbf{q} = p \cdot \mathbf{q} + B \quad (3.71)$$

Chapter 4

Results

4.1 Polarizability

In this section the results of the model are displayed and compared with the ones obtained in the quasi-static regime featured in [63].

Quasi-static-polarizability is modelled as follows.

$$\alpha_{QS}(\omega) = 4\pi a^3 \varepsilon_2 \frac{\varepsilon_1(\omega) - \varepsilon_2}{\varepsilon_1(\omega) + 2\varepsilon_2} \quad (4.1)$$

a : radius of the mgNP; ε_1 : permittivity of the metal; ε_2 : Drude permittivity of the gain medium, obtained by Lorentzian model [?].

Mie polarizability is obtained with.

$$\alpha_{Mie}(\omega) = 6\pi i \frac{\tilde{a}_1}{k^3} \quad (4.2)$$

\tilde{a}_1 : first scattering Mie coefficient obtained with the model, corresponding to dipolar mode; $k = \frac{2\pi n_2}{\lambda}$, n_2 : refractive index of the host, λ : wavelength corresponding to the exciting field frequency.

The following figure shows the evolution of these polarizabilities in a silver nanoparticle with radius 1 nm by adding different levels of gain to the system: no gain, some gain, and enough gain to drive the system into emission ($G > G_{th}$). The gain medium's central frequency was chosen to match ω_{pl} . The left column depicts time dependency for one chosen frequency, while the right column shows the corresponding steady state spectrum.

With no gain added, 4.1 (a-b) shows the perfect correspondence between quasi-static and Mie polarizability. Both polarizabilities converge to the steady state value showed in 4.1 (b).

In 4.1 (c-d) the pump was turned on by adding some gain below the emission threshold $G = 0.5G_{th}$ to the system. It exhibits the same correspondence in the time domain, and also when it reaches the steady state.

In 4.1 (e-f) gain was added to drive the system into emission, $G = 1.1G_{th}$. Correspondence with 4.1 (f) can not be found, since the system will no longer reach a steady state. However, 4.1 (e) still exhibits time evolution correspondence between both polarizabilities calculated frequency by frequency. As was first noted by [63], [65], a negative imaginary part of the steady state polarizability aligns with an emissive regime, which manifests in 4.1 (e)

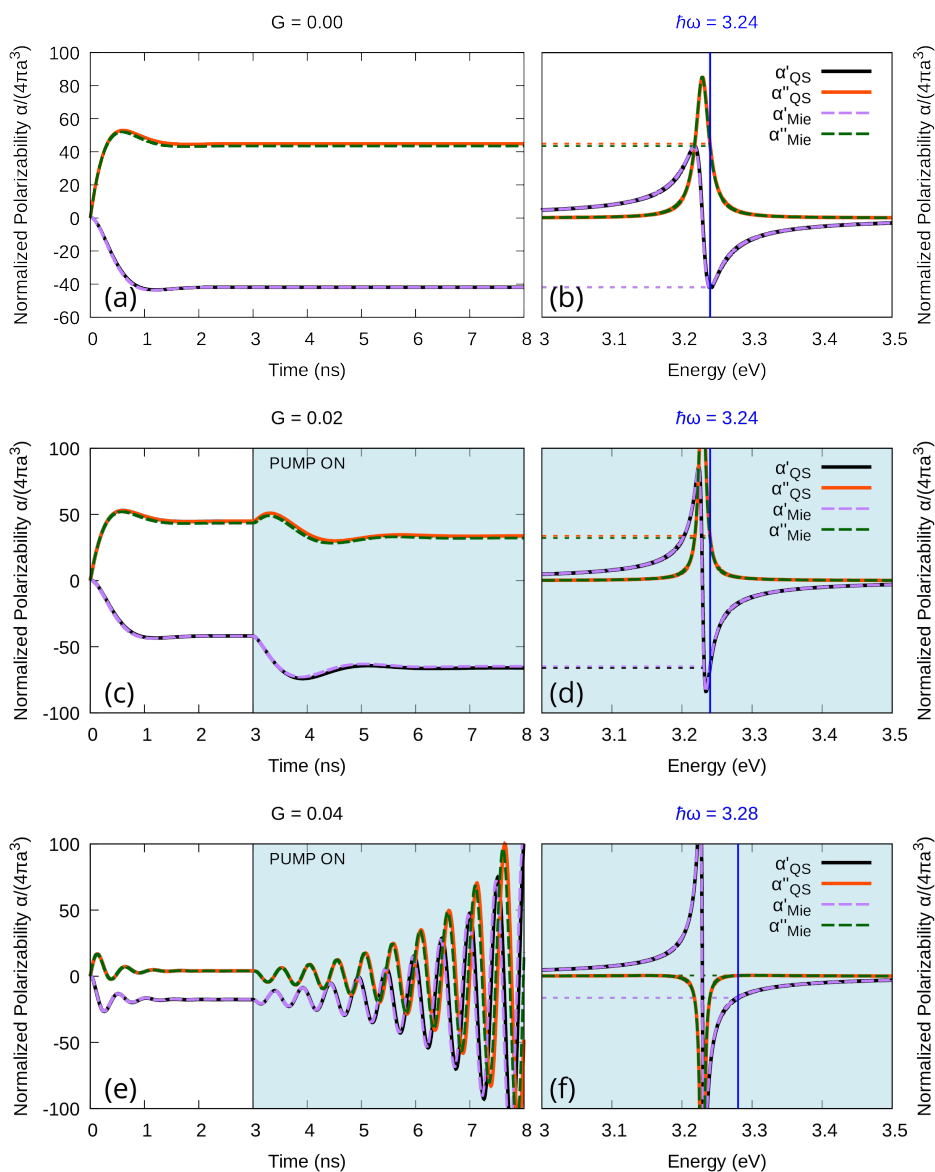


Figure 4.1: Real and imaginary part of the Polarizability of a silver nanoparticle of radius 1 nm in water enriched with a gain medium with emission central frequency $\hbar\omega_{21} = 3.23$ eV and emission width $\Delta = 0.15$ eV. (a,b): No gain is added to the system. (c,d): Some gain is included, but the system remains sub-emissive ($G = 0.5 \cdot G_{th}$). (e,f): Enough gain is included to drive the system to the emissive regime ($G = 1.1 \cdot G_{th}$). (a,c,e): Time dependence of the polarizability for a single frequency; (b,d,f): corresponding steady state spectrum.

In 4.2 polarizabilities are modelled for a particle of 10 nm radius..

It can clearly be observed how the quasi-static model can no longer accurately match the Mie polarizability in either the time evolution frequency by frequency, or the corresponding steady state spectrum. It can be seen though, that the Mie polarizability does converge to the same value in the steady state 4.2 (b,d) with no gain, and with some gain added to the system.

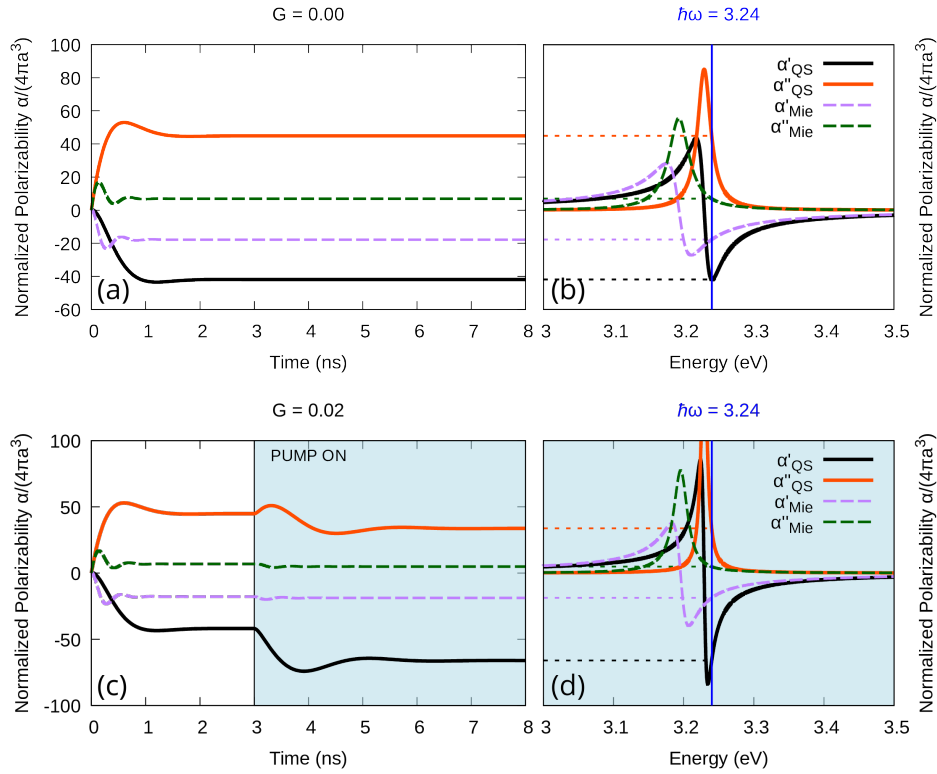


Figure 4.2: Real and imaginary part of the Polarizability of a silver nanoparticle of radius 10 nm in water enriched with a gain medium with emission central frequency $\hbar\omega_{21} = 3.23$ eV and emission width $\Delta = 0.15$ eV. (a,b): No gain is added to the system. (c,d): Some gain is included, but the system remains sub-emissive ($G = 0.5 \cdot G_{th}$). (a,c): Time dependence of the polarizability for a single frequency; (b,d): corresponding steady state spectrum.

4.2 Mie coefficients

As discussed previously in -3, each coefficient of the Mie expansion a_n corresponds to a resonance mode. Considering the new model reaches beyond the quasi-static limit, modes higher than the dipolar one can be detected.

In 4.3 the time evolution of the dipolar and quadrupolar coefficients a_1 , a_2 of the scattered field, and corresponding steady state are calculated for a mgNP of 10 nm radius when no gain is added to the system.

One can see that though the quasi-static approach no longer accurately describes the system, the dipolar mode is still dominant, as the amplitude of resonance of the quadrupolar mode is almost two hundred times smaller. Both reach a steady state.

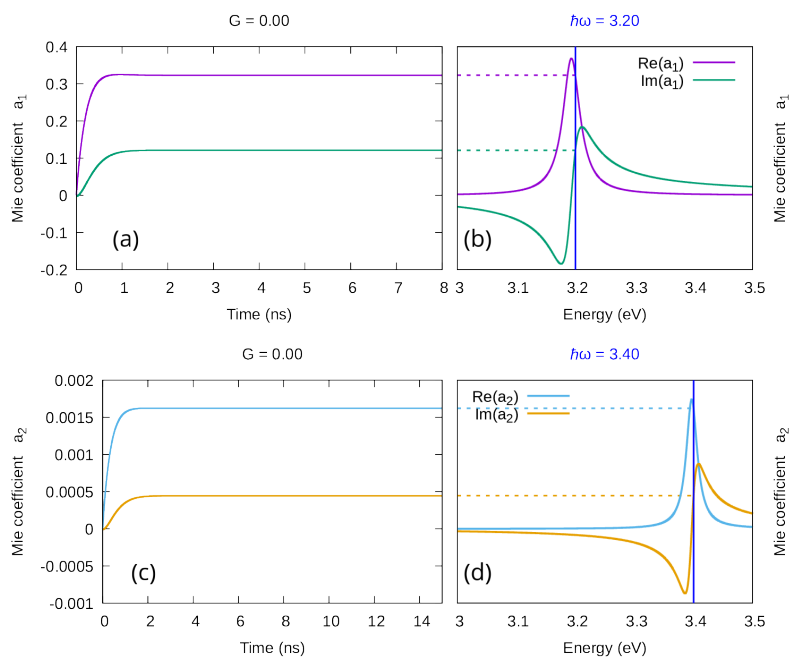


Figure 4.3: Real and imaginary parts of the first two coefficients of the Mie expansion of the scattered field for a silver nanoparticle of radius 10 nm in water, when no gain is included in the system. (a,b): coefficient a_1 dipolar mode; (c,d): coefficient a_2 quadrupolar mode; (a,c): time dependencies for a single frequency; (b,d): corresponding steady state spectrum.

4.3 Higher mode enhancing

Up next, some gain below the emission threshold was added to the system. The central emission frequency ω_{21} was chosen to match the resonance frequency of each mode. In 4.4 (a-d) the emission center line matches that of the dipolar mode, while in 4.4 (e-h) it matches the quadrupolar mode.

It can be observed comparing 4.3 (b) with 4.4(b), and 4.3 (d) with 4.4 (d) that by matching the emission central frequency to the dipolar resonance, there is a threefold enhance in the dipolar mode, while the quadrupolar mode remains virtually unchanged.

By contrast, when the emission center line matches the quadrupolar mode, comparing 4.3 (b) with 4.4 (f), and 4.3 (d) with 4.4 (h), almost a tenfold increase can be observed for the quadrupolar mode a_2 , while the dipolar one is enhanced by very little. This result illustrates how by choosing the right center-line, higher-order modes can be significantly amplified until they become non-negligible. Another notable observation is the heightened sensitivity of the quadrupolar mode compared to the dipolar one when increasing gain.

On another note, the concept of *gain-driven mode-cascade* discussed in [63] pertains to the occurrence of a physical phenomenon known as spatial hole burning SHB when gain levels beyond G_{th} are injected into the system. When gain is fully consumed in the vicinity of the nanosphere, a cascade of modes ensues (higher-order resonances are activated). This phenomenon can occur even for very small particles and can no longer be accurately modelled by the quasi-static approximation. While we also discuss mode enhancement in this section, these are certainly two different phenomena that merit individual analysis.

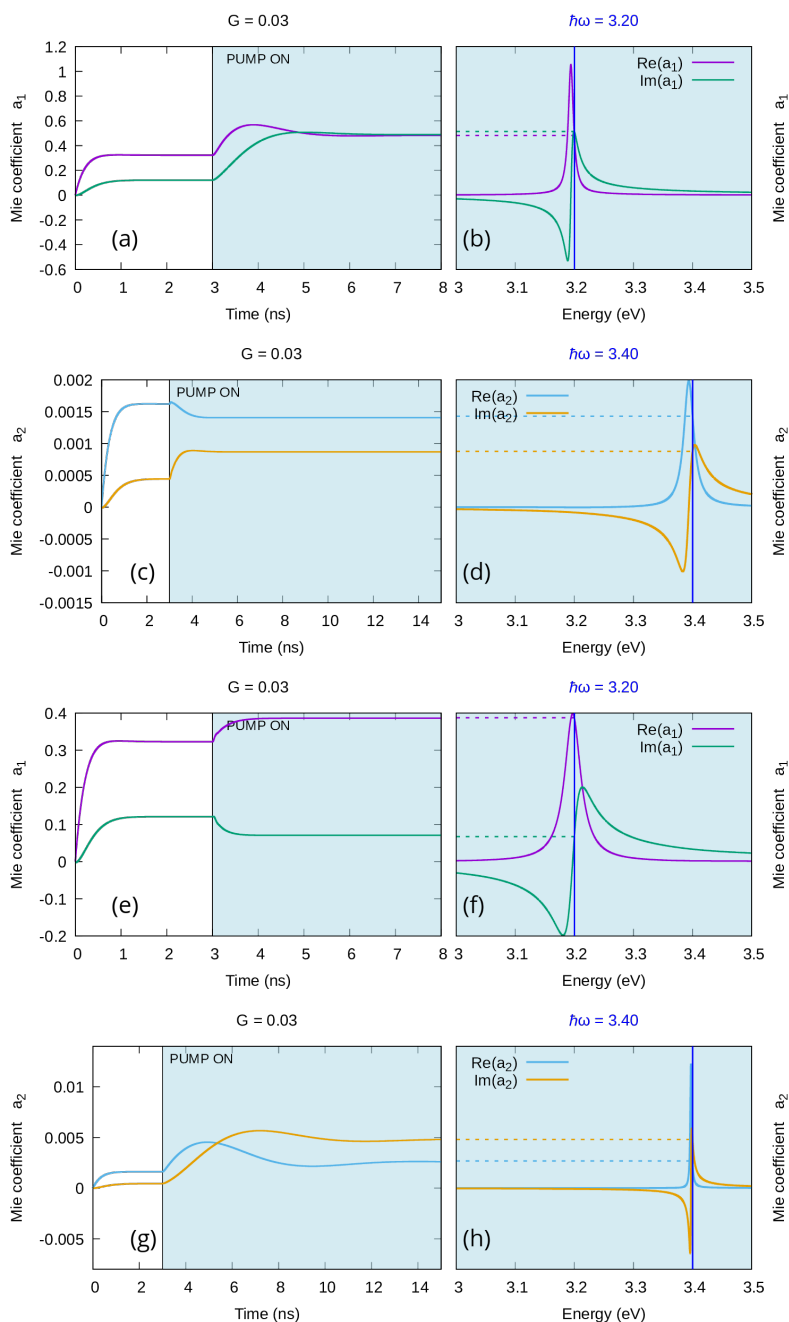


Figure 4.4: Real and imaginary part of the first two coefficients of the Mie expansion of the scattered field for a silver nanoparticle of radius 10 nm in water enriched with a gain medium below the emission threshold $G = 0.03$ with emission bandwidth $\Delta = 0.15$ eV. **(a–d)**: the emission central frequency $\hbar\omega_{21} = 3.19$ eV was chosen to correspond to the resonance frequency of the dipolar mode. **(e–h)**: the emission central frequency $\hbar\omega_{21} = 3.4$ eV was chosen to correspond to the resonance frequency of the quadrupolar mode. **(a,b,e,f)**: coefficient a_1 dipolar mode; **(c,d,g,h)**: coefficient a_2 quadrupolar mode; **(a,c,e,g)**: time dependencies for a single frequency; **(b,d,f,h)**: corresponding steady state spectrum.

4.4 Higher mode gain-driven emission

Lastly, as was mentioned before in 4.1, an emissive regime emerges when enough gain is added to the system to make the imaginary part of the polarizability negative. In the same manner, the emissive regime can be found for any of the coefficients and in turn for any of the resonance modes by adding a quantity of gain $G > G_{th}$ to the medium.

In 4.5 the quantity of gain chosen is $G = 0.4$, while for the quadrupolar mode the emission threshold was estimated to be $G_{th} = 0.03495$. It is clearly observed in 4.5 (a) that the coefficient a_2 oscillates widely and can no longer reach a steady state, proving it has entered the emissive regime.

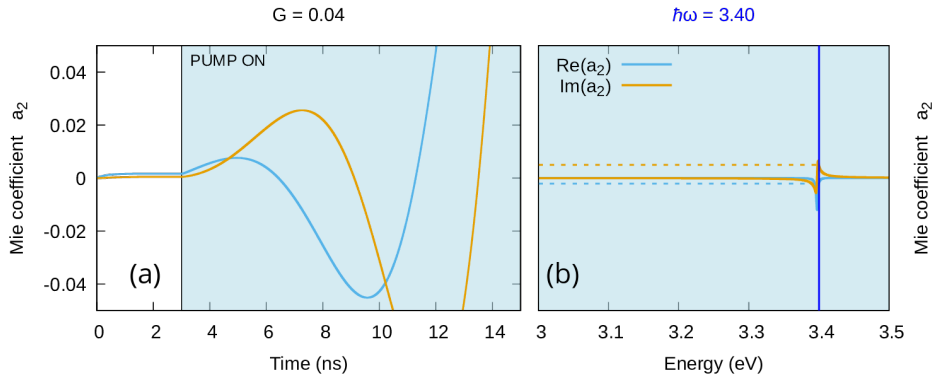


Figure 4.5: Real and imaginary part quadrupolar coefficient of the Mie expansion of the scattered field for a silver nanoparticle of radius 10 nm in water enriched with a gain medium above the emission threshold $G = 0.04$ with emission bandwidth $\Delta = 0.15$ eV. Here, the emission central frequency $\hbar\omega_{21} = 3.4$ eV was chosen to correspond to the resonance frequency of the quadrupolar mode. (a): Time dependencies for a single frequency; (b): corresponding steady state spectrum.

4.5 Gain driven field sculpting

As a result of the full description of the time evolution of the fields reached in 3, a visual representation of the scattered field through a mgNP can be produced. Each Mie coefficient is combined with the vector spherical harmonics to produce the images presented in this section. In 4.7 we have a spherical NP of radius 10 nm with no gain added to the system. A dipolar mode can clearly be observed even though the emission center-line corresponds to the quadrupole.

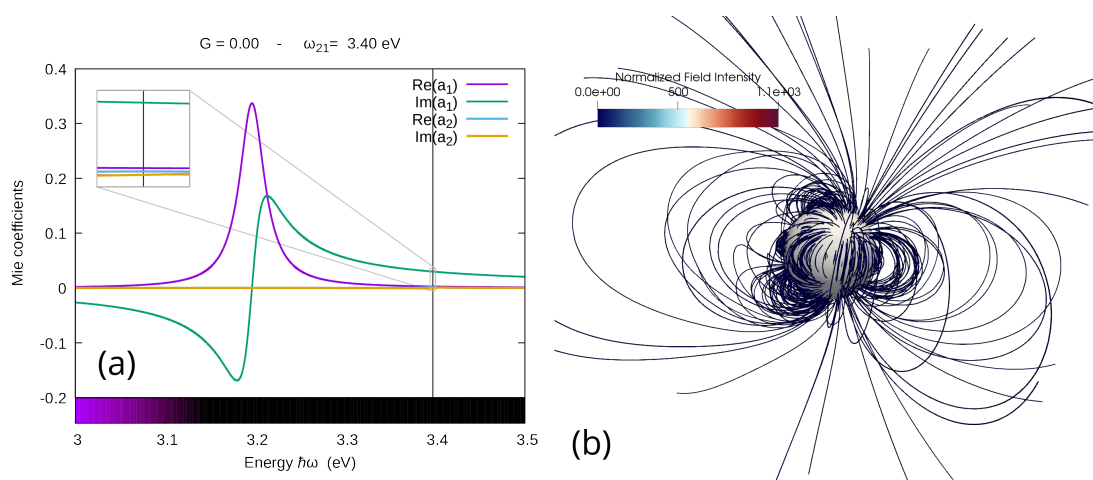


Figure 4.6: (a) spectra for the real and imaginary part of the first two coefficients of the Mie expansion of the scattered field for a silver nanoparticle of radius 10 nm in water when no gain is added to the system, the inset in the upper left corner is a zoom around the resonance frequency of the second coefficient; (b) streamlines of the scattered field calculated for the quadrupolar central frequency $h\omega = 3.4$ eV, the colorbar range here is the same as fig. 4.8(b).

In the next figure it is made more evident how by choosing the quadrupole emission center-line, incrementing the level of gain quantity in the system G leads to enhancement of the quadrupolar coefficient. $G_s = 0.03334$ is calculated by the bisection method.

In the following figure, the enhanced effect of incrementing the gain level becomes more evident when choosing the quadrupole emission center-line.

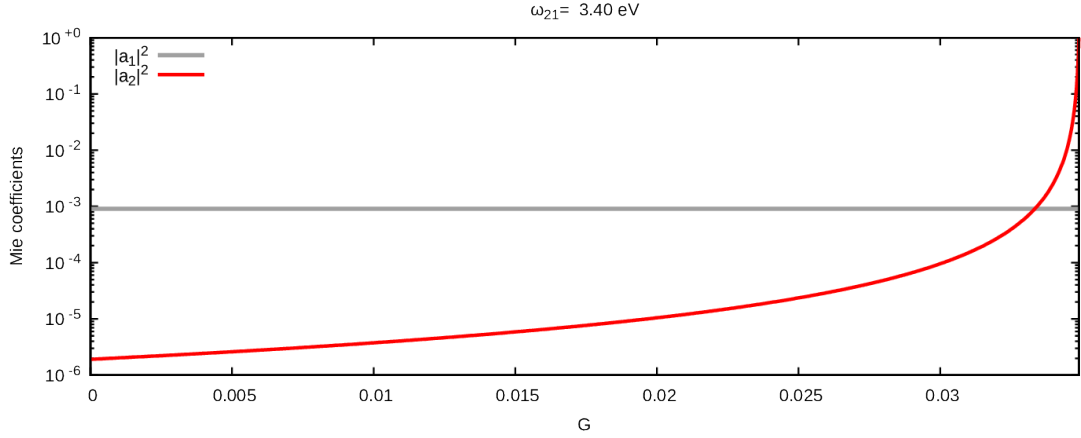


Figure 4.7: Behavior of the square modulus of the first two coefficients of the Mie expansion for the scattered field at the quadrupolar mode frequency; calculated for a silver nanoparticle of radius 10 nm in water as a function of the gain quantity G present in the system. Here the emission central frequency was chosen to correspond to the resonance frequency of the quadrupolar mode.

Consequently, after enhancing the quadrupolar mode with a sub-emissive quantity of gain around its resonance frequency coefficient a_2 is greater than a_1 . Therefore, the scattered field has a dominantly quadrupolar shape.

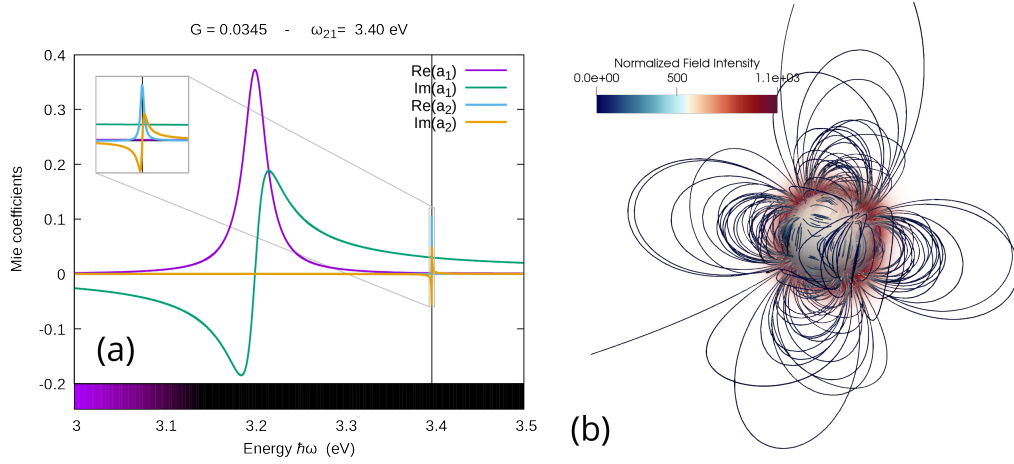


Figure 4.8: (a) spectra for the real and imaginary part of the first two coefficients of the Mie expansion of the scattered field for a silver nanoparticle of radius 10 nm in water enriched with a gain medium below the emission threshold $G = 0.03$ with emission bandwidth $\Delta = 0.15$ eV. Here the emission central frequency $\hbar\omega_{21} = 3.4$ eV was chosen to correspond to the resonance frequency of the quadrupolar mode, the inset in the upper left corner is a zoom around the resonance frequency of the second coefficient; (b): streamlines of the scattered field calculated for the quadrupole central frequency, the colorbar range here is the same as fig. 4.6(b).

Chapter 5

Discussion

We initiate the discussion by clarifying that the reason the present model can not yet characterize the emissive regime concerns the time and space dependency of population inversion N that appears after SHB kicks in. Nevertheless, reporting on the evolution of the coefficients in the emissive regime when $G > G_{th}$ was not necessary to validate the model so it was not presented in the previous chapter.

As was shown in 4.1, results obtained with the Mie model were validated by selecting a sufficiently small particle that should satisfy both the quasi-static and Mie approaches, and perfect correspondence in both frequency-by-frequency time evolution and steady state spectra were found.

Through the implementation of the model presented in this research, we are able to describe nanoparticles of realistic sizes. Studying bigger particles unveils more interesting phenomena whose characterization was beyond reach with quasi-static approach.

We also discuss how an emission regime G_{th} can be identified for any of the modes by the same principle used with the polarizability 4.4. Sufficient gain must be added to the system until the imaginary part of the chosen coefficient turns negative. Emission regimes for any mode can now be predicted.

Previously, higher modes could only be activated by the *gain-driven mode-cascade*, and while this phenomena could happen in very small particles, there was no control over which modes activate. Now, as was revealed in 4.3 by electing an appropriate center-line for the gain media frequency corresponding to the mode's resonance G_{th} , we can essentially enhance any mode, effectively sculpting the scattered field with sub-emissive levels of gain.

Lastly, given that the time evolution of the coefficients for the expansion of the scattered field is determined, visual representations of the resulting scattered fields can be produced 4.5.

Research is still needed to fully characterize metallic LSP's, specially concerning emissive regimes where population inversion does not remain constant in space and time. Moreover, as disclosed in 4.3, a full explanation regarding the sensitivity that higher modes exhibit to gain levels of the system is also necessary, as currently we can only hypothesize why the dipolar mode presents a threefold enhancement while the quadrupolar one a tenfold. Future work ought to elucidate this phenomena, and go in the direction of fully describing the mode cascade, potentially encompassing particles of any size.

Chapter 6

Conclusions

In this study, we have introduced a newfound model that enables the characterization of nanoparticles of any size, overcoming the constraints inherent to the quasi-static regime, and providing a more realistic approach. As discussed in earlier sections, there is still ample opportunity for improvement of the method, as well as for further exploration of the *gain-driven-mode-cascade*.

Nonetheless, our present research reinforces the necessity of integrating Mie theory to advance in the direction of a full description of metal LSP's. A valuable new insight is that by choosing the proper emission center-line, any mode can be enhanced by the gain medium, even in particles exclusively believed to sustain dipolar modes. This newfound phenomenon opens up the opportunity to customize and sculpt the electromagnetic field scattered by a particle without requiring emissive levels of gain. In addition, the tools developed in this study have enabled us to present a dynamic and visual representation of the evolution of the field.

Bibliography

- [1] Nicolò Maccaferri, Sophie Meuret, Nikolay Kornienko, and Deep Jariwala. Speeding up Nanoscience and Nanotechnology with Ultrafast Plasmonics. *Nano Letters*, 2020.
- [2] S.A. Maier. *Plasmonics: fundamentals and applications*. Springer Verlag, 2007.
- [3] M. A. Noginov, G. Zhu, A. M. Belgrave, R. Bakker, V. M. Shalaev, E. E. Narimanov, S. Stout, E. Herz, T. Suteewong, and U. Wiesner. Demonstration of a spaser-based nanolaser. *Nature*, 460(7259):1110–1112, August 2009. Number: 7259 Publisher: Nature Publishing Group.
- [4] R. H. Ritchie. Surface Plasmons in Solids. *Surf. Sci.*, 34:1–19, 1973.
- [5] A. Abdolvand, A. Podlipensky, G. Seifert, and H. Graener. Fine optical structuring in glass with embedded elliptical silver nanoparticles using dc electric field. pages 347–, June 2005.

- [6] K.-H. Su, Q.-H. Wei, X. Zhang, J.J. Mock, D.R. Smith, and S. Schultz. Surface plasmon coupling between two nano Au particles. 1:279–282 vol.2, August 2003.
- [7] K. Lance Kelly, Eduardo Coronado, Lin Lin Zhao, and George C. Schatz. The Optical Properties of Metal Nanoparticles: The Influence of Size, Shape, and Dielectric Environment. *The Journal of Physical Chemistry B*, 107(3):668–677, January 2003. Publisher: American Chemical Society.
- [8] N. M. Lawandy. Localized Surface Plasmon Singularities in Amplifying Media. *Appl. Phys. Lett.*, 85:5040–5042, 2004.
- [9] Gustav Mie. Beiträge zur Optik trüber Medien, speziell kolloidaler Metallösungen. *Annalen der Physik*, 330(3):377–445, 1908.
- [10] Arnim Henglein. Physicochemical properties of small metal particles in solution: “microelectrode” reactions, chemisorption, composite metal particles, and the atom-to-metal transition. *The Journal of Physical Chemistry*, 92(24):6689–6696, 1988.
- [11] U. Kreibig, R. Fässler, J. Meyer, M. Vollmer, W. Frank, L. Genzel, and S. Schlör. Size-dependent electron–hole pair generation in very small metal particles. *Surface Science*, 324(1-3):321–327, 1995.
- [12] R. A. Alvarez-Puebla, C. Márquez, S. Sánchez-Cortés, F. J. García de Abajo, and L. M. Liz-Marzán. Optical absorption spectra of nanometric gold particles. *The Journal of Physical Chemistry B*, 102(5):937–941, 1998.

- [13] Stephan Link and Mostafa A. El-Sayed. Spectral properties and relaxation dynamics of surface plasmon electronic oscillations in gold and silver nanodots and nanorods. *The Journal of Physical Chemistry B*, 103(40):8410–8426, 1999.
- [14] Amanda J. Haes and Richard P. Van Duyne. Shape-controlled synthesis of silver nanoparticles for surface-enhanced raman spectroscopy. *Chemistry of Materials*, 11(2):482–489, 1999.
- [15] S. A. Maier, M. L. Brongersma, P. G. Kik, and H. A. Atwater. Plasmonics—a route to nanoscale optical devices. *Advanced Materials*, 14(11):823–829, 2002.
- [16] E. Prodan, P. Nordlander, and N. J. Halas. Plasmon hybridization in spherical nanoparticles. *The Journal of Chemical Physics*, 120(12):5444–5454, 2004.
- [17] L. Novotny and B. Hecht. Principles of nano-optics. *Cambridge University Press*, 2006.
- [18] R. A. Alvarez-Puebla, L. M. Liz-Marzán, and P. Mulvaney. Electromagnetic field enhancement in plasmonic nanospheres: A theoretical study. *Journal of Quantitative Spectroscopy and Radiative Transfer*, 110(10):1086–1094, 2009.
- [19] CJ DeSantis and DJ Masiello. Thermal effects in plasmonic nanoparticles: Physics and applications. *Materials Today*, 16(3):86–95, 2013.
- [20] Y. Yang and P. Mühlischlegel. Analytical solutions for plasmon modes of a coupled nanosphere dimer. *The Journal of Chemical Physics*, 142(8):084109, 2015.
- [21] Y. Fang, M. Sun, Y. Li, and W. Lu. Fundamentals and applications of plasmonic nanoparticles. *CRC Press*, 2019.

- [22] F. Liu and P. Guyot-Sionnest. Mechanism of silver (i)-assisted growth of gold nanorods and bipyramids. *The Journal of Physical Chemistry B*, 109(42):18609–18615, 2005.
- [23] L. Gou, C.J. Murphy, and J. Gao. High yield synthesis of single crystal gold nanospheres. *Journal of Materials Chemistry*, 15(20):2167–2172, 2005.
- [24] Y. Wang, X. Wei, Y. Wang, and J. Zhao. Controlled synthesis of monodisperse silver nanospheres: The effect of reaction temperature. *Colloids and Surfaces A: Physicochemical and Engineering Aspects*, 407:94–100, 2012.
- [25] U. Vainio, T. Venäläinen, and H. Tenhu. Effect of temperature on the stability and aggregation kinetics of gold nanoparticles stabilized by hydrophobized poly(ethylene imine). *Langmuir*, 26(5):3355–3362, 2010.
- [26] X. Sun and Y. Li. Colloidal carbon spheres and their core/shell structures with noble-metal nanoparticles. *Angewandte Chemie International Edition*, 43(5):597–601, 2004.
- [27] Y. Chen, Z. Li, and C. Wang. Synthesis and thermal stability of monodisperse gold nanorods and nanospheres. *Nano Research*, 3(4):244–254, 2006.
- [28] NR Jana, L Gearheart, and CJ Murphy. Seed-mediated synthesis of spherical gold nanoparticles in high purity and with plasmon resonances tunable through the visible and near-infrared. *The Journal of Physical Chemistry B*, 105(19):4065–4067, 2001.

- [29] CB Murray, CR Kagan, and MG Bawendi. Synthesis and characterization of monodisperse nanocrystals and close-packed nanocrystal assemblies. *Annual review of materials science*, 30(1):545–610, 2000.
- [30] Daizy Philip, Gopinathan Anilkumar Unni, SA Aromal, VK Vidhu, and BS Murraya. Green synthesis of spherical gold nanoparticles by using dioscorea bulbifera tuber extract. *Green Chemistry Letters and Reviews*, 7(3):257–263, 2014.
- [31] Younan Xia, Yujie Xiong, Byungkwon Lim, and Sara E Skrabalak. Shape-controlled synthesis of metal nanocrystals: simple chemistry meets complex physics? *Angewandte Chemie International Edition*, 48(1):60–103, 2008.
- [32] Jongnam Park, Kwangjin An, Yongsu Hwang, Jongnam Park, Hyeonho Noh, Seungyeon Kwon, Hyonbin Na, Youngjoo Kim, and Jinho Park. Facile synthesis of monodisperse iron oxide nanoparticles by thermal decomposition of iron carboxylate salts in organic solvents. *Nanoscale research letters*, 4(7):693–698, 2009.
- [33] Qian Zhang, Nana Li, James Goebel, Zhenda Lu, and Yadong Yin. Scalable and green synthesis of monodisperse silver nanoparticles using green tea extract for biomedical applications. *ACS Sustainable Chemistry & Engineering*, 4(1):59–65, 2016.
- [34] Xueyan Zheng, Huaqiang Xu, and Zhiguang Guo. A facile and scalable synthesis of monodisperse gold nanoparticles using polyethyleneimine as a reducing agent. *Journal of colloid and interface science*, 367(1):147–152, 2012.

- [35] E. Plum, VA Fedotov, P. Kuo, DP Tsai, and NI Zheludev. Towards the lasing spaser: controlling metamaterial optical response with semiconductor quantum dots. *Optics Express*, 17(10):8548–8550, 2009.
- [36] Pei Song, Jian-Hua Wang, Miao Zhang, Fan Yang, Hai-Jie Lu, Bin Kang, Jing-Juan Xu, and Hong-Yuan Chen. Three-level spaser for next-generation luminescent nanoprobe. *Science Advances*, 4(8):eaat0292, August 2018.
- [37] Jagdeep Shah. Ultrafast luminescence and nonlinear optical properties of semiconductor microcrystallites. *The Journal of Physical Chemistry*, 93(2):744–752, 1989.
- [38] Robert J Moerland, Ad Legendijk, and Alfons van Blaaderen. Spectroscopy and gain in dye-doped polymer optical fiber amplifiers. *Applied physics letters*, 59(13):1481–1483, 1991.
- [39] D Waters, D Fittinghoff, J Squier, K DeLong, R Trebino, and K Wilson. High-gain, high-fidelity optical parametric chirped pulse amplifier system using spatiotemporally shaped pump pulses. *Optics letters*, 21(9):674–676, 1996.
- [40] Mark P Andrews, Louis R Bradshaw, and Andrew J Ouder Kirk. Optical amplification and lasing in dye-doped polymer thin films. *Journal of Applied Physics*, 83(4):1877–1883, 1998.
- [41] A. Fang, T. Koschny, and C.M. Soukoulis. Self-consistent calculations of loss-compensated fishnet metamaterials. *Physical Review B*, 82(12):121102, 2010.

- [42] S. Xiao, V.P. Drachev, A.V. Kildishev, X. Ni, U.K. Chettiar, H.K. Yuan, and V.M. Shalaev. Loss-free and active optical negative-index metamaterials. *Nature*, 466(7307):735–738, 2010.
- [43] A. Chipouline, J. Petschulat, A. Tuennermann, T. Pertsch, C. Menzel, C. Rockstuhl, F. Lederer, and V. A. Fedotov. Multipole model for metamaterials with gain: from nano-laser to quantum metamaterials. pages 807000–807000–9, 2011.
- [44] S.Y. Liu, J. Li, F. Zhou, L. Gan, and Z.Y. Li. Efficient surface plasmon amplification from gain-assisted gold nanorods. *Optics letters*, 36(7):1296–1298, 2011.
- [45] S. Wuestner, A. Pusch, K.L. Tsakmakidis, J.M. Hamm, and O. Hess. Overcoming losses with gain in a negative refractive index metamaterial. *Physical review letters*, 105(12):127401, 2010.
- [46] PM Bolger, W. Dickson, AV Krasavin, L. Liebscher, SG Hickey, D.V. Skryabin, and AV Zayats. Amplified spontaneous emission of surface plasmon polaritons and limitations on the increase of their propagation length. *Optics letters*, 35(8):1197–1199, 2010.
- [47] G. Strangi, A. De Luca, S. Ravaine, M. Ferrie, and R. Bartolino. Gain induced optical transparency in metamaterials. *Applied Physics Letters*, 98(25):251912, 2011.
- [48] A. De Luca, M. P. Grzelczak, I. Pastoriza-Santos, L. M. Liz-Marzán, M. La Deda, M. Striccoli, and G. Strangi. Dispersed and Encapsulated Gain Medium

- in Plasmonic Nanoparticles: a Multipronged Approach to Mitigate Optical Losses. *ACS Nano*, 5(7):5823–5829, 2011.
- [49] Melissa Infusino, Antonio De Luca, Alessandro Veltri, Carmen Vázquez-Vázquez, Miguel Correa-Duarte, Rakesh Dhama, and Giuseppe Strangi. Loss-Mitigated Collective Resonances in Gain-Assisted Plasmonic Mesocapsules. *ACS Photonics*, 1(4):371–376, 2014.
- [50] A. Rahimi Rashed, A. De Luca, R. Dhama, A. Hosseinzadeh, M. Infusino, M. El Kabbash, S. Ravaine, R. Bartolino, and G. Strangi. Battling absorptive losses by plasmon-exciton coupling in multimeric nanostructures. *RSC Advances*, 5(66):53245–53254, 2015.
- [51] M. I. Stockman. Spasers explained. *Nature Photonics*, 2(6):327–329, 2008.
- [52] N.I. Zheludev, S.L. Prosvirnin, N. Papasimakis, and V.A. Fedotov. Lasing Spaser. *Nature Photon.*, 2:351–354, 2008.
- [53] Martin T. Hill, Milan Marell, Eunice S. P. Leong, Barry Smalbrugge, Youcai Zhu, Minghua Sun, Peter J. van Veldhoven, Erik Jan Geluk, Fouad Karouta, Yok-Siang Oei, Richard Nötzel, Cun-Zheng Ning, and Meint K. Smit. Lasing in metal-insulator-metal sub-wavelength plasmonic waveguides. *Optics Express*, 17(13):11107–11112, June 2009. Publisher: Optica Publishing Group.
- [54] Rupert F. Oulton, Volker J. Sorger, Thomas Zentgraf, Ren-Min Ma, Christopher Gladden, Lun Dai, Guy Bartal, and Xiang Zhang. Plasmon lasers at deep subwavelength scale. *Nature*, 461(7264):629–632, October 2009. Number: 7264 Publisher: Nature Publishing Group.

- [55] Ekaterina I. Galanzha, Robert Weingold, Dmitry A. Nedosekin, Mustafa Sarimollaoglu, Jacqueline Nolan, Walter Harrington, Alexander S. Kuchyanov, Roman G. Parkhomenko, Fumiya Watanabe, Zeid Nima, Alexandru S. Biris, Alexander I. Plekhanov, Mark I. Stockman, and Vladimir P. Zharov. Spaser as a biological probe. *Nature Communications*, 8:1–7, 2017. Publisher: Nature Publishing Group.
- [56] Catherine Alix-Panabières and Klaus Pantel. Biological labels: Here comes the spaser. *Nature Materials*, 16(8):790–791, 2017. Publisher: Nature Publishing Group.
- [57] Shaimaa I. Azzam, Alexander V. Kildishev, Ren-Min Ma, Cun-Zheng Ning, Rupert Oulton, Vladimir M. Shalaev, Mark I. Stockman, Jia-Lu Xu, and Xiang Zhang. Ten years of spasers and plasmonic nanolasers. *Light: Science & Applications*, 9(1):90, May 2020. Number: 1 Publisher: Nature Publishing Group.
- [58] A. Veltri and A. Aradian. Optical response of a metallic nanoparticle immersed in a medium with optical gain. *Physical Review B*, 85(11):115429, 2012.
- [59] A. De Luca, M. Ferrie, S. Ravaine, M. La Deda, M. Infusino, A.R. Rashed, A. Veltri, A. Aradian, N. Scaramuzza, and G. Strangi. Gain functionalized core-shell nanoparticles: the way to selectively compensate absorptive losses. *J. Mater. Chem.*, 2012.

- [60] Vincenzo Caligiuri, Luigia Pezzi, Alessandro Veltri, and Antonio De Luca. Resonant Gain Singularities in 1D and 3D Metal/Dielectric Multilayered Nanostructures. *ACS Nano*, 11(1):1012–1025, jan 2017.
- [61] Paolo Polimeno, Francesco Patti, Melissa Infusino, Jonathan Joel Sanchez, Maria Antonia Iati, Rosalba Saija, Giovanni Volpe, Onofrio M. Marago, and Alessandro Veltri. Gain-Assisted Optomechanical Position Locking of Metal/Dielectric Nanoshells in Optical Potentials. *ACS Photonics*, 2020.
- [62] Paolo Polimeno, Francesco Patti, Melissa Infusino, Maria Antonia Iatì, Rosalba Saija, Giovanni Volpe, Onofrio M. Maragò, and Alessandro Veltri. Optical trapping of gain-assisted plasmonic nano-shells: theoretical study of the optical forces in a pumped regime below the emission threshold. In Kishan Dholakia and Gabriel C. Spalding, editors, *Optical Trapping and Optical Micromanipulation XVIII*, volume 11798, pages 170 – 177. International Society for Optics and Photonics, SPIE, 2021.
- [63] Alessandro Veltri, Arkadi Chipouline, and Ashod Aradian. Multipolar, time-dynamical model for the loss compensation and lasing of a spherical plasmonic nanoparticle spaser immersed in an active gain medium. *Scientific Reports*, 6(September):33018, sep 2016.
- [64] C. F. Bohren and D. R. Huffman. *Absorption and Scattering of Light by Small Particles*. WILEY-VCH Verlag GmbH & Co. KGaA, 1998.
- [65] Karen Caicedo, Andres Cathey, Melissa Infusino, Ashod Aradian, and Alessandro Veltri. Gain-driven singular resonances in active core-shell and

nano-shell plasmonic particles. *Journal of the Optical Society of America B*, 39(1):107, jan 2022.

Appendix A

Optical Bloch equations

Our model for the time dynamic evolution of the polarization in the gain medium makes use of the Optical Bloch equations describing the interaction between an atom modeled as a two level system with a classical electric field. For the sake of completeness, we will present in the following a derivation of these equations.

The Hamiltonian of a two level system where the quantum leap between the two levels is $\Delta E = \hbar\omega_{21}$ can be modeled as:

$$\hat{H}_A = -\frac{\hbar}{2}\omega_{21}\hat{\sigma}_z \quad (\text{A.1})$$

where $\hat{\sigma}_z$ is the third Pauli matrix. This is simply because in the Pauli matrices

notation the only two possible statuses $|1\rangle$ and $|1\rangle$ are represented by the vectors:

$$|1\rangle = (1, 0), \quad (\text{A.2})$$

$$|2\rangle = (0, 1); \quad (\text{A.3})$$

so, using the definition presented in A.1 we get:

$$E_1 = \hat{H}_A|1\rangle = -\frac{\hbar}{2}\omega_{21} \begin{pmatrix} 1 & 0 \\ 0 & -1 \end{pmatrix} (1, 0) = -\frac{\hbar}{2}\omega_{21}(1, 0) = -\frac{\hbar}{2}\omega_{21}|1\rangle, \quad (\text{A.4})$$

$$E_2 = \hat{H}_A|2\rangle = -\frac{\hbar}{2}\omega_{21} \begin{pmatrix} 1 & 0 \\ 0 & -1 \end{pmatrix} (0, 1) = \frac{\hbar}{2}\omega_{21}(0, 1) = \frac{\hbar}{2}\omega_{21}|2\rangle; \quad (\text{A.5})$$

providing the exact ΔE required by our model.

To obtain the Hamiltonian of interaction between the atom and the electric field we now have to consider the classical coupling term between a dipole and an electric field:

$$\hat{H}_I = -\hat{\mathbf{D}} \cdot \mathbf{E} \quad (\text{A.6})$$

where the atom dipole moment is expressed as the dipole operator $\hat{\mathbf{D}}$. Finding a suitable model for $\hat{\mathbf{D}}$ (possibly in terms of Pauli matrices) corresponds to having a good model of this interaction term.

A.1 The operator dipole moment

If we consider the parity operator $\hat{\mathcal{P}}$ we note that it has the property:

$$\hat{\mathcal{P}}\hat{\mathbf{R}}\hat{\mathcal{P}}^\dagger = -\hat{\mathbf{R}}, \quad (\text{A.7})$$

where $\hat{\mathbf{R}}$ is the position operator. Using this property we can show that:

$$\hat{\mathcal{P}}\hat{\mathbf{R}} = \hat{\mathcal{P}}\hat{\mathbf{R}}\hat{\mathcal{P}}^\dagger\hat{\mathcal{P}} = -\hat{\mathbf{R}}\hat{\mathcal{P}} \quad \Rightarrow \quad \hat{\mathcal{P}}\hat{\mathbf{R}} = -\hat{\mathbf{R}}\hat{\mathcal{P}}, \quad (\text{A.8})$$

meaning that, when applied to the position operator, the parity operator produces an inversion of space. In order to build a realistic dipole moment operator, it is mandatory that the parity operator have the same effect on it, meaning that:

$$\hat{\mathcal{P}}\hat{\mathbf{D}} = -\hat{\mathbf{D}}\hat{\mathcal{P}}. \quad (\text{A.9})$$

This is the same as the property:

$$\{\hat{\mathbf{D}}, \hat{\mathcal{P}}\} = 0. \quad (\text{A.10})$$

where $\{\hat{\mathbf{D}}, \hat{\mathcal{P}}\}$ is the anti-commutator of $\hat{\mathbf{D}}$ and $\hat{\mathcal{P}}$. If we now project this anti-commutator in the base $\{|1\rangle, |2\rangle\}$ we have:

$$\langle i|\{\hat{\mathbf{D}}, \hat{\mathcal{P}}\}|j\rangle = 0 \quad \Rightarrow \quad \langle i|\hat{\mathcal{P}}\hat{\mathbf{D}}|j\rangle + \langle i|\hat{\mathbf{D}}\hat{\mathcal{P}}|j\rangle = 0. \quad (\text{A.11})$$

The Hamiltonian A.1 is even and thus commutes with $\hat{\mathcal{P}}$, therefore $|1\rangle$ and $|1\rangle$ are also eigenvectors of $\hat{\mathcal{P}}$ which means that $\hat{\mathcal{P}}|i\rangle = \pi_i|i\rangle$ and $\hat{\mathcal{P}}|j\rangle = \pi_j|j\rangle$. Consequently equation A.11 reduces to:

$$(\pi_i + \pi_j)\langle i|\hat{\mathbf{D}}|j\rangle = 0, \quad (\text{A.12})$$

for this to be true, we must have:

$$\langle i|\hat{\mathbf{D}}|j\rangle = 0 \quad \text{when} \quad \pi_i + \pi_j \neq 0; \quad (\text{A.13})$$

$$\langle i|\hat{\mathbf{D}}|j\rangle \neq 0 \quad \text{when} \quad \pi_i + \pi_j = 0. \quad (\text{A.14})$$

However being π_i and π_j eigenvalues of $\hat{\mathcal{P}}$, they can only be ± 1 meaning that if $i = j$ we have that $\pi_i + \pi_j = \pm 2 \neq 0$, this implies that $\langle 1|\hat{\mathbf{D}}|1\rangle = 0$ and that $\langle 2|\hat{\mathbf{D}}|2\rangle = 0$. On the other hand if $i \neq j$ we have that $\pi_i + \pi_j = 0$ which implies that $\langle 1|\hat{\mathbf{D}}|2\rangle \neq 0$ and that $\langle 2|\hat{\mathbf{D}}|1\rangle \neq 0$.

We can now use the completeness of the base $\{|1\rangle, |2\rangle\}$

$$\hat{I} = |1\rangle\langle 1| + |2\rangle\langle 2|, \quad (\text{A.15})$$

to calculate

$$\begin{aligned} \hat{\mathbf{D}} &= \hat{I}\hat{\mathbf{D}}\hat{I} = (|1\rangle\langle 1| + |2\rangle\langle 2|)\hat{\mathbf{D}}(|1\rangle\langle 1| + |2\rangle\langle 2|) = \\ &= |1\rangle\langle 1|\hat{\mathbf{D}}|2\rangle\langle 2| + |2\rangle\langle 2|\hat{\mathbf{D}}|1\rangle\langle 1| \end{aligned}$$

meaning that:

$$\hat{\mathbf{D}} = \langle 1|\hat{\mathbf{D}}|2\rangle|1\rangle\langle 2| + \langle 2|\hat{\mathbf{D}}|1\rangle|2\rangle\langle 1|. \quad (\text{A.16})$$

We will now ask for this operator to be Hermitian (i. e. $\langle 1|\hat{\mathbf{D}}|2\rangle = \langle 1|\hat{\mathbf{D}}|2\rangle^*$) and we chose its phase so that $\langle 1|\hat{\mathbf{D}}|2\rangle$ is real. This way equation A.16 turns into:

$$\hat{\mathbf{D}} = \langle 1|\hat{\mathbf{D}}|2\rangle [|1\rangle\langle 2| + |2\rangle\langle 1|]. \quad (\text{A.17})$$

Here we notice that the operator $|1\rangle\langle 2| + |2\rangle\langle 1|$ is the Pauli matrix $\hat{\sigma}_x$ while the vector factor $\langle 1|\hat{\mathbf{D}}|2\rangle$ can be identified as the classical dipole moment $\boldsymbol{\mu}$, this means that finally the dipole moment operator can be written as

$$\hat{\mathbf{D}} = \boldsymbol{\mu} \cdot \hat{\sigma}_x. \quad (\text{A.18})$$

Consequently the interaction Hamiltonian will be:

$$\hat{H}_I = -\boldsymbol{\mu} \cdot \mathbf{E} \hat{\sigma}_x \quad (\text{A.19})$$

while the Hamiltonian defining our problem is the sum of \hat{H}_A and \hat{H}_I , meaning:

$$\hat{H} = -\frac{1}{2}\hbar\omega_{21}\hat{\sigma}_z - \boldsymbol{\mu} \cdot \mathbf{E}\hat{\sigma}_x \quad (\text{A.20})$$

A.2 Polarization of the material

We can now describe our material as a population of two level systems with transition dipole moment $\boldsymbol{\mu}$ with different orientations and the same modulus. If we write the dipole moment of one of these atoms specifying its orientation in polar coordinates, we have:

$$\boldsymbol{\mu} = \mu(\sin \theta \cos \phi, \sin \theta \sin \phi, \cos \theta) \quad (\text{A.21})$$

To calculate the corresponding polarization \mathbf{P} , we have to recall that:

$$\mathbf{P} = \frac{d\boldsymbol{\mu}}{dV} \Rightarrow \mathbf{P}dV = d\boldsymbol{\mu} \Rightarrow \int_V \mathbf{P}dV = \int_{\boldsymbol{\mu}} d\boldsymbol{\mu}, \quad (\text{A.22})$$

if the particle density n over the volume V is sufficiently uniform, the last one can be written as:

$$\mathbf{P}V = \int_{\boldsymbol{\mu}} d\boldsymbol{\mu} = \frac{N\mu}{4\pi} \int_{4\pi} (\sin \theta \cos \phi, \sin \theta \sin \phi, \cos \theta)d\Omega, \quad (\text{A.23})$$

where N is the number of atoms in the volume V . This can be written as:

$$\mathbf{P} = \int_{\boldsymbol{\mu}} d\boldsymbol{\mu} = \frac{n\mu}{4\pi} \int_{4\pi} (\sin \theta \cos \phi, \sin \theta \sin \phi, \cos \theta)d\Omega. \quad (\text{A.24})$$

It is evident that this integral gives $(0, 0, 0)$ which is consistent with the polarization provided by a population of uniformly distributed classical dipoles. This evidences that the very existence of this polarization depends on the quantum-mechanics-driven probability that these dipoles appear as a consequence of a tran-

sition between the two levels.

The quantum mechanics equivalent of a single dipole μ is the expected value $\langle \hat{\mathbf{D}} \rangle$ over the ket $|\Psi\rangle$ representing the state of the system. Taking this into account, equation A.24 turns into:

$$\mathbf{P} = \frac{n}{4\pi} \int_{4\pi} \langle \Psi | \hat{\mathbf{D}} | \Psi \rangle d\Omega \quad (\text{A.25})$$

As the \hat{D} operator gives the value of the dipole moment of a given state Ψ . For the two level atom with states $|1\rangle$ and $|2\rangle$, the general state can be written as:

$$|\Psi\rangle = C_1 |1\rangle + C_2 |2\rangle \quad (\text{A.26})$$

if we now recall that the dipole moment operator can also be expressed as:

$$\hat{\mathbf{D}} = \boldsymbol{\mu} [|1\rangle \langle 2| + |2\rangle \langle 1|] \quad (\text{A.27})$$

and use the orthogonality $\langle 1|2\rangle = \langle 2|1\rangle = 0$, we have:

$$\begin{aligned} \langle \Psi | \hat{\mathbf{D}} | \Psi \rangle &= [C_1^* \langle 1| + C_2^* \langle 2|] \hat{\mathbf{D}} [C_1 |1\rangle + C_2 |2\rangle] \\ &= \boldsymbol{\mu} [C_1^* \langle 1| + C_2^* \langle 2|] [|1\rangle \langle 2| + |2\rangle \langle 1|] [C_1 |1\rangle + C_2 |2\rangle] \\ &= \boldsymbol{\mu} [C_1^* \langle 2| + C_1^* \langle 1|2\rangle \langle 1| + C_2^* \langle 2|1\rangle \langle 2| + C_2^* \langle 1|] [C_1 |1\rangle + C_2 |2\rangle] \\ &= \boldsymbol{\mu} [C_1^* \langle 2| + C_2^* \langle 1|] [C_1 |1\rangle + C_2 |2\rangle] \\ &= \boldsymbol{\mu} [C_1^* \langle 2| + C_2^* \langle 1|] [C_1 |1\rangle + C_2 |2\rangle] \end{aligned} \quad (\text{A.28})$$

where the only surviving terms are:

$$\langle \Psi | \hat{\mathbf{D}} | \Psi \rangle = \boldsymbol{\mu} [C_1^* C_2 + C_1 C_2^*] \quad (\text{A.29})$$

we now define $C_1^* C_2 : \rho_{21}$ and $C_1 C_2^* : \rho_{12}$ as the diagonal elements of the density matrix, then

$$\langle \Psi | \hat{\mathbf{D}} | \Psi \rangle = \boldsymbol{\mu} [\rho_{21} + \rho_{12}] \quad (\text{A.30})$$

Going back to equation A.25 and since $\rho_{21} = \rho_{12}^*$

$$\mathbf{P} = \frac{n}{4\pi} \int_{4\pi} \boldsymbol{\mu} [\rho_{12} + \rho_{12}^*] d\Omega \quad (\text{A.31})$$

A.2.1 Time evolution of the density matrix

As one can see in equation A.31, the time evolution of polarization in a medium that can be modeled as a population of two-levels system atoms, is determined by the time evolution of the elements of the density matrix defined as $\rho_{ij} = \langle i | \hat{\rho} | j \rangle$ where $\hat{\rho} = |\Psi\rangle\langle\Psi|$ is the density operator associated to the state $|\Psi\rangle$.

The time evolution of $\hat{\rho}$ is defined as:

$$\frac{\partial \hat{\rho}}{\partial t} = \frac{1}{i\hbar} [\hat{H}, \hat{\rho}], \quad (\text{A.32})$$

using the Hamiltonian obtained in A.1, we can calculate

$$\begin{aligned}\langle 1 | [\hat{H}, \hat{\rho}] | 2 \rangle &= \langle 1 | [\hat{H} \hat{\rho}] | 2 \rangle - \langle 1 | [\hat{\rho} \hat{H}] | 2 \rangle \\ &= -\hbar\omega_{21}\rho_{12} - \mu \cdot \hat{E}[\rho_{22} - \rho_{11}]\end{aligned}\tag{A.33}$$

then we obtain

$$\frac{\partial \rho_{12}}{\partial t} = \frac{1}{i\hbar} \{-\hbar\omega_{21}\rho_{12} - \mu \cdot \hat{E}[\rho_{22} - \rho_{11}]\}\tag{A.34}$$

similarly,

$$\frac{\partial \rho_{21}}{\partial t} = \frac{1}{i\hbar} \{-\hbar\omega_{21}\rho_{21} - \mu \cdot \hat{E}[\rho_{11} - \rho_{22}]\}\tag{A.35}$$

$$\frac{\partial \rho_{11}}{\partial t} = \frac{1}{i\hbar} \{-\mu \cdot \hat{E}[\rho_{21} - \rho_{12}]\}\tag{A.36}$$

$$\frac{\partial \rho_{22}}{\partial t} = \frac{1}{i\hbar} \{-\mu \cdot \hat{E}[\rho_{12} - \rho_{21}]\}\tag{A.37}$$

If we now define population inversion as

$$N = \rho_{22} - \rho_{11}\tag{A.38}$$

We note that since the rate of variation must remain constant between the two levels, $\dot{\rho}_{11} + \dot{\rho}_{22} = 0$.

We can obtain the first optical Bloch equation by subtracting A.36 from A.37

$$\frac{dN}{dt} = \frac{2i}{\hbar} [\rho_{12} - \rho_{21}] \mu \cdot \hat{E}\tag{A.39}$$

The second optical Bloch equation is obtained by reorganizing A.34

$$\frac{d\rho_{12}}{dt} - i\omega_{21}\rho_{12} = \frac{iN}{\hbar}\boldsymbol{\mu} \cdot \hat{E}. \quad (\text{A.40})$$

Taking into account the energy relaxation time τ_1 due to the interaction with an external thermal reservoir placed at an energy corresponding to a population inversion \tilde{N} and the phase relaxation time, due to the interaction with other atoms in the system and with an external thermal reservoir, equations A.39 and A.40 become:

$$\frac{d\rho_{12}}{dt} - \left(i\omega_{21} - \frac{1}{\tau_2}\right)\rho_{12} = \frac{iN}{\hbar}\boldsymbol{\mu} \cdot \hat{E}. \quad (\text{A.41})$$

$$\frac{dN}{dt} + \frac{N - \tilde{N}}{\tau_1} = \frac{2i}{\hbar}[\rho_{12} - \rho_{21}]\boldsymbol{\mu} \cdot \hat{E} \quad (\text{A.42})$$

A.3 Code for the temporal evolution of the fields

After compilation, the code can be run with the command `./ult_coeffs ω` , where ω must be specified in eV. This code calculates the Mie coefficients a_n .

```

1 #include <iostream>
2 #include <iomanip>
3 #include <fstream>
4 #include <sstream>
5 #include <stdlib.h>
6 #include <boost/math/special_functions/spherical_harmonic.hpp>
7 #include <armadillo>
8 #include "cup_eV.H"

```

```

9 #include "mathNN.H"
10 #include <sys/types.h>
11 #include <algorithm>
12 #include <complex_bessel.h>
13 #include <ctime>
14 #include <string>
15 #include <stdlib.h>
16 #include <pwd.h>
17
18
19 #define eV2j 1.60217733000103e-19
20 /** Compila con:
21 g++ ultimo_coeffs.cxx      -o ult_coeffs    -lgsl -lgslcblas -lm -
22     lcomplex_bessel -larmadillo
23 **/
24 using namespace std;
25 using namespace sp_bessel;
26 complex<double> img=complex<double> (0,1.);
27 // Bessel Functions.
28 std::complex<double> j (double order, std::complex<double> x){
29     return sph_besselJ(order,x);
30 }
31 std::complex<double> h1 (double order, std::complex<double> x){
32     return sph_hankelH1(order, x);
33 }
34
35 // Riccati-Bessel Functions.
36 std::complex<double> RBj (double order, std::complex<double> x){
37     return x*sph_besselJ(order,x);

```

```

38     }
39 std::complex<double> RBj_prime (double order, std::complex<double> x){
40     return (x*sph_besselJ(order-1,x)-order*sph_besselJ(order,x));
41     }
42 std::complex<double> RBh (double order, std::complex<double> x){
43     return x*sph_hankelH1(order, x);
44     }
45 std::complex<double> RBh_prime (double order, std::complex<double> x){
46     return (x*sph_hankelH1(order-1,x)-order*sph_hankelH1(order,x));
47     }
48
49 //E_n
50 std::complex<double> E(int n, std::complex <double> E0){
51     return pow(img,n)*(2.*n+1.)*E0/(n*(n+1.));
52 }
53 std::complex<double> Gwiggly(double order, double G, std::complex <double> E0,
54     double T2){
55     std::complex<double> GG;
56     GG = -img*G*E(order, E0)/T2;
57     if (norm(GG)<=1.e-60) GG = std::complex<double> (1.e-60, 1.e-60);
58     return GG;
59 }
60 std::complex<double>** gimme_p(int order, double ome, std::complex <double> k,
61     std::complex <double> x, std::complex <double> m){
62     std::complex<double>** p;
63     p = new std::complex<double>*[6];
64     for (int j = 0; j < 6; j++) p[j] = new std::complex<double>[6];
65
66     p[0][0] = -(RBj_prime(order, m*x)*pow(ome, 2)*RBh_prime(order, x))/(j(order
67     , m*x)*k*pow(m,2)*x*RBh_prime(order, x)-h1(order, x)*k*RBj_prime(order, m*x

```

```

)*x);
65 p[0][1] = 0;
66 p[0][2] = 0;
67 p[0][3] = (pow(RBj_prime(order, m*x),2)*pow(ome, 2))/(j(order, m*x)*k*pow(m
,3)*x*RBh_prime(order, x)-h1(order, x)*k*m*RBj_prime(order, m*x)*x);
68 p[0][4] = (RBj_prime(order, m*x)*pow(ome, 2)*RBj_prime(order, x))/(j(order,
m*x)*k*pow(m,2)*x*RBh_prime(order, x)-h1(order, x)*k*RBj_prime(order, m*x)
*x);
69 p[0][5] = (j(order, m*x)*pow(m,2)*RBj_prime(order, x)-j(order, x)*RBj_prime
(order, m*x))/(j(order, m*x)*pow(m,2)*RBh_prime(order, x)-h1(order, x)*
RBj_prime(order, m*x));
70
71 p[1][0] = (pow(h1(order, x),2)*pow(ome,2)*x)/(j(order, m*x)*k*RBh_prime(
order, x)-h1(order, x)*k*RBj_prime(order, m*x));
72 p[1][1] = 0;
73 p[1][2] = 0;
74 p[1][3] = -(h1(order, x)*j(order, m*x)*pow(ome,2)*x)/(j(order, m*x)*k*
RBh_prime(order, x)-h1(order, x)*k*RBj_prime(order, m*x));
75 p[1][4] = -(h1(order, x)*j(order, x)*pow(ome,2)*x)/(j(order, m*x)*k*
RBh_prime(order, x)-h1(order, x)*k*RBj_prime(order, m*x));
76 p[1][5] = -(h1(order, x)*RBj_prime(order, x)-j(order, x)*RBh_prime(order, x)
)/(j(order, m*x)*RBh_prime(order, x)-h1(order, x)*RBj_prime(order, m*x));
77
78 p[2][0] = -(h1(order, x)*j(order, m*x)*pow(ome,2)*x)/(j(order, m*x)*k*
RBh_prime(order, x)-h1(order, x)*k*RBj_prime(order, m*x));
79 p[2][1] = (pow(j(order, m*x),2)*pow(ome,2)*x)/(j(order, m*x)*k*RBh_prime(
order, x)-h1(order, x)*k*RBj_prime(order, m*x));
80 p[2][2] = (j(order, m*x)*j(order, x)*pow(ome,2)*x)/(j(order, m*x)*k*
RBh_prime(order, x)-h1(order, x)*k*RBj_prime(order, m*x));
81 p[2][3] = 0;

```

```

82 p[2][4] = 0;
83 p[2][5] = (j(order, m*x)*RBj_prime(order, x)-j(order,x)*RBj_prime(order, m*
x))/(j(order, m*x)*RBh_prime(order, x)-h1(order, x)*RBj_prime(order, m*x));
84
85 p[3][0] = (m*pow(ome, 2)*pow(RBh_prime(order, x),2))/(j(order, m*x)*k*pow(m
,2)*x*RBh_prime(order, x)-h1(order, x)*k*RBj_prime(order, m*x)*x);
86 p[3][1] = -(RBj_prime(order, m*x)*pow(ome, 2)*RBh_prime(order, x))/(j(order
, m*x)*k*pow(m,2)*x*RBh_prime(order, x)-h1(order, x)*k*RBj_prime(order, m*x
)*x);
87 p[3][2] = -(m*pow(ome, 2)*RBh_prime(order, x)*RBj_prime(order, x))/(j(order
, m*x)*k*pow(m,2)*x*RBh_prime(order, x)-h1(order, x)*k*RBj_prime(order, m*x
)*x);
88 p[3][3] = 0;
89 p[3][4] = 0;
90 p[3][3] = -(h1(order, x)*m*RBj_prime(order, x)-j(order, x)*m*RBh_prime(
order, x))/(j(order, m*x)*pow(m,2)*RBh_prime(order, x)-h1(order, x)*
RBj_prime(order, m*x));
91
92 return p;
93 }
94
95 std::complex<double>** coeffsMatriz(int order, double ome, std::complex <double
> k, std::complex <double> x, std::complex <double> m, std::complex <
double> GG, std::complex <double> E0, std::complex<double> OmeH, std:::
complex<double> OmeP, std:::complex<double> GamP){
96
97     std::complex<double>** M = 0;
98     M = new std::complex<double>*[6];
99     for (int j = 0; j < 6; j++) M[j] = new std::complex<double>[6];
100

```

```
101     std::complex<double>** p;
102     p = new std::complex<double>*[6];
103     for (int j = 0; j < 6; j++) p[j] = new std::complex<double>[6];
104
105     p=gimme_p(order,ome,k, x, m);
106     M[0][0] = OmeH+GG*p[0][0];
107     M[0][1] = GG*p[0][1];
108     M[0][2] = GG*p[0][2];
109     M[0][3] = GG*p[0][3];
110     M[0][4] = GG*p[0][4];
111     M[0][5] = GG*p[0][5];
112
113     M[1][0] = GG*p[1][0];
114     M[1][1] = OmeH+GG*p[1][1];
115     M[1][2] = GG*p[1][2];
116     M[1][3] = GG*p[1][3];
117     M[1][4] = GG*p[1][4];
118     M[1][5] = GG*p[1][5];
119
120     M[2][0] = GamP*p[2][0];
121     M[2][1] = GamP*p[2][1];
122     M[2][2] = OmeP+GamP*p[2][2];
123     M[2][3] = GamP*p[2][3];
124     M[2][4] = GamP*p[2][4];
125     M[2][5] = GamP*p[2][5];
126
127     M[3][0] = GamP*p[3][0];
128     M[3][1] = GamP*p[3][1];
129     M[3][2] = GamP*p[3][2];
130     M[3][3] = OmeP+GamP*p[3][3];
```

```

131     M[3][4] = GamP*p[3][4];
132     M[3][5] = GamP*p[3][5];
133
134     M[4][0] = 0;
135     M[4][1] = 0;
136     M[4][2] = 0;
137     M[4][3] = 0;
138     M[4][4] = OmeH;
139     M[4][5] = 0;
140
141     M[5][0] = 0;
142     M[5][1] = 0;
143     M[5][2] = 0;
144     M[5][3] = 0;
145     M[5][4] = 0;
146     M[5][5] = OmeH;
147
148     return M;
149 }
150
151 std::complex<double> gimme_a(int order, double ome, std::complex<double> k,
    std::complex<double> x, std::complex<double> m, std::complex<double> *q,
    std::complex<double> E0){
152     std::complex<double> a;
153
154     std::complex<double>** p;
155     p = new std::complex<double>*[6];
156     for (int j = 0; j < 6; j++) p[j] = new std::complex<double>[6];
157     p=gimme_p(order,ome,k, x, m);
158

```

```

159     a=p[0][0]*q[0]+p[0][1]*q[1]+p[0][2]*q[2]+p[0][3]*q[3]+p[0][4]*q[4]+p[0][5]*
      q[5];
160     return a;
161 }
162
163 std::complex<double>* inhomogeneousB( int order, double ome, std::complex <
      double> k, std::complex <double> x, std::complex <double> m, std::complex
      <double> GG, std::complex <double> E0, std::complex<double> GamP){
164     std::complex<double>* B = 0;
165     B = new std::complex<double>[6];
166
167     std::complex<double>** p;
168     p = new std::complex<double>*[6];
169     for (int j = 0; j < 6; j++) p[j] = new std::complex<double>[6];
170
171     p=gimme_p(order,ome,k, x, m);
172
173     B[0] = GG*p[0][6]*E0;
174     B[1] = GG*p[1][6]*E0;
175     B[2] = GamP*p[2][6]*E0;
176     B[3] = GamP*p[3][6]*E0;
177     B[4] = GG*E0;
178     B[5] = GG*E0;
179
180     return B;
181 }
182
183
184 int main (int argc, char** argv){
185     if (argv[1]==0){

```



```

186     cout<<endl<<" Usage: "<<argv[0]<<" <omega in eV>"<<endl<<endl;
187     exit(0);
188 }
189 //constants
190 double ome, ome_21, omemi, omema, T2, gamd, lam, eps_b, eps_inf, G=0,
ome_eV=3.2;
191 complex<double> eps1, eps2, m, x, n1, n2, k,k1, Nf=1, N=-1, E0=1;
192 complex <double> OmeH, OmeP, GamP, GG;
193 int order=1;
194 char mtl[16], mdl[16], sol[16], active[16];
195
196 ome_eV=atof(argv[1]);
197
198 nanosphere ns;
199 ns.init();
200
201 fstream nano;
202 nano.open("in/nanosphere_eV.dat",ios::in);
203 nano>>ns.r1>>ns.Dome>>ns.ome_0>>ns.G>>omemi>>omema>>mtl>>mdl>>active>>sol;
204
205
206 ns.r1=ns.r1*1.e-9;
207 ns.set_metal(mtl,mdl,1);
208 ns.set_active(active);
209
210 eps_b=ns.set_host(sol);
211 eps_inf=ns.eps_inf;
212 eps1 = ns.metal(ome_eV);
213 eps2 = ns.active(ome_eV, eps_b);
214

```

```

215 ome=ome_eV/ns.Ome_p;
216 ome_21=ns.ome_0/ns.Ome_p;
217 gamd=.5*ns.Gam_d/ns.Ome_p;
218 T2=2.*ns.Ome_p/ns.Dome;
219
220 n1=sqrt(eps1);
221 n2=sqrt(eps2);
222 m=n1/n2;
223
224 lam =h*cc/(ns.r1*ome_eV*eV2j);
225 k = 2.*ns.pi*n2/lam;
226 k1=m*k;
227 x=k;
228
229 OmeH= img*(ome-ome_21)-1/T2;
230 OmeP= ome*(ome+2.*img*gamd)/(2.*(gamd-img*ome));
231 GamP= 1./(2.*(gamd-img*ome));
232
233
234 GG=Gwiggly(order, ns.G, EO, T2);
235 complex <double> **coefis=coeffsMatriz(order, ome, k, x, m, GG, EO, OmeH,
OmeP, GamP);
236 complex <double> *inhomog=inhomogeneousB(order, ome, k, x, m, GG, EO, GamP)
;
237
238 complex<double> *kap;
239 kap = new std::complex<double>[6];
240
241 fstream egva;
242 egva.open("out/eigenvalues.dat", std::ios::out);

```

```

243
244 kap = eigenvalues(coefis,6);
245
246 egva<<" "<<setw(8)<<setiosflags (ios::left)<<ome_eV<< // 1
    ome
247     "\t"<<setw(11)<<setiosflags (ios::left)<<ns.Ome_p*real(kap[0])<< // 2
    Re(kap1)
248     "\t"<<setw(11)<<setiosflags (ios::left)<<ns.Ome_p*imag(kap[0])<< // 3
    Im(kap1)
249     "\t"<<setw(11)<<setiosflags (ios::left)<<ns.Ome_p*real(kap[1])<< // 4
    Re(kap2)
250     "\t"<<setw(11)<<setiosflags (ios::left)<<ns.Ome_p*imag(kap[1])<< // 5
    Im(kap2)
251     "\t"<<setw(11)<<setiosflags (ios::left)<<ns.Ome_p*real(kap[2])<< // 6
    Re(kap3)
252     "\t"<<setw(11)<<setiosflags (ios::left)<<ns.Ome_p*imag(kap[2])<< // 7
    Im(kap3)
253     "\t"<<setw(11)<<setiosflags (ios::left)<<ns.Ome_p*real(kap[3])<< // 6
    Re(kap4)
254     "\t"<<setw(11)<<setiosflags (ios::left)<<ns.Ome_p*imag(kap[3])<< // 7
    Im(kap4)
255     "\t"<<setw(11)<<setiosflags (ios::left)<<ns.Ome_p*real(kap[4])<< // 6
    Re(kap5)
256     "\t"<<setw(11)<<setiosflags (ios::left)<<ns.Ome_p*imag(kap[4])<< // 7
    Im(kap5)
257     "\t"<<setw(11)<<setiosflags (ios::left)<<ns.Ome_p*real(kap[5])<< // 6
    Re(kap6)
258     "\t"<<setw(11)<<setiosflags (ios::left)<<ns.Ome_p*imag(kap[5])<< // 7
    Im(kap6)
259 endl;

```

```

260
261     fstream fnct, miec;
262     fnct.open("out/anlfunc.dat", std::ios::out);
263     miec.open("out/anlmiec.dat", std::ios::out);
264
265     double omep = eV2j*ns.Ome_p/h; //converto in Hz
266     double t, T = 10., dt=1.; // tiempo total en picosegundos
267     complex<double> *qss, *q, **EVE, *C, a1, d1;
268     T=T*omep*1.e-12; // in ome_p
269     int i, Nt=T/dt;
270     qss = new std::complex<double>[6];
271     EVE = new std::complex<double>*[6];
272     for(int i = 0; i < 6; i++)
273         EVE[i] = new std::complex<double>[6];
274     C = new std::complex<double>[6];
275
276     q = new std::complex<double>[6];
277     for(int i = 0; i < 6; i++) q[i] = std::complex<double> (0., 0.);
278
279     kap = eigenvalues(coefis,6);
280     EVE = eigenvectors(coefis, 6);
281     qss = steady_state_solution(coefis, inhomog, 6);
282     C = constantes(coefis, inhomog, q, 6);
283     i=0;
284     while (i<=Nt){
285         t=i*dt;
286         i++;
287         for(int ii = 0; ii < 6; ii++)
288             q[ii] = qss[ii] + C[0]*EVE[ii][0]*exp(kap[0]*t)
289                 + C[1]*EVE[ii][1]*exp(kap[1]*t)

```

```

290         + C[2]*EVE[ii][2]*exp(kap[2]*t)
291         + C[3]*EVE[ii][3]*exp(kap[3]*t)
292         + C[4]*EVE[ii][4]*exp(kap[4]*t)
293         + C[5]*EVE[ii][5]*exp(kap[5]*t);
294
295     fnct<<" " <<setw(8)<<setiosflags (ios::left)<<t/omep*1.e+12<< // 1
time (ps)
296     "\t" <<setw(13)<<setiosflags (ios::left)<<real(q[0])<< // 2
Re(alph)
297     "\t" <<setw(13)<<setiosflags (ios::left)<<imag(q[0])<< // 3
Im(alph)
298     "\t" <<setw(13)<<setiosflags (ios::left)<<real(q[1])<< // 4
Re(beta)
299     "\t" <<setw(13)<<setiosflags (ios::left)<<imag(q[1])<< // 5
Im(beta)
300     "\t" <<setw(13)<<setiosflags (ios::left)<<real(q[2])<< // 6
Re(kappa)
301     "\t" <<setw(13)<<setiosflags (ios::left)<<imag(q[2])<< // 7
Im(kappa)
302     "\t" <<setw(13)<<setiosflags (ios::left)<<real(q[3])<< // 8
Re(delta)
303     "\t" <<setw(13)<<setiosflags (ios::left)<<imag(q[3])<< // 9
Im(delta)
304     "\t" <<setw(13)<<setiosflags (ios::left)<<real(q[4])<< // 10
Re(eta)
305     "\t" <<setw(13)<<setiosflags (ios::left)<<imag(q[4])<< // 11
Im(eta)
306     "\t" <<setw(13)<<setiosflags (ios::left)<<real(q[5])<< // 10
Re(zeta)
307     "\t" <<setw(13)<<setiosflags (ios::left)<<imag(q[5])<< // 11

```

```
Im(zeta)
308     endl;
309
310     miec<<" " <<setw(8)<<setiosflags (ios::left)<<t/omep*1.e+12<< // 1
time (ps)
311     "\t"<<setw(13)<<setiosflags (ios::left)<<real(a1)<< // 2 Re
(a1)
312     "\t"<<setw(13)<<setiosflags (ios::left)<<imag(a1)<< // 3 Im
(a1)
313     endl;
314 }
315
316 a1 = gimme_a(order,ome, k, x, m, qss, E0)/E(order,E0);
317 cout<<"a["<<order<<" ] = "<<a1<<endl;
318 return 0;
319 }
```